Graz University of Technology

Doctoral Thesis

Adaptive Calibration of Frequency Response Mismatches in Time-Interleaved Analog-to-Digital Converters

Shahzad Saleem

Signal Processing and Speech Communication Laboratory
Graz University of Technology, Austria

First Examiner:
Univ.-Prof. Dr. Gernot Kubin
Graz University of Technology, Austria

Second Examiner:
Prof. Dr. Svante Signell
KTH - Royal Institute of Technology, Sweden

Co-Advisor:
Dr. Christian Vogel
Telecommunications Research Center (FTW), Vienna, Austria

Graz, December 2010

STATUTORY DECLARATION

I declare that I have authored this thesis independently, that I have not used other than the declared sources / resources and that I have explicitly marked all material which has been quoted either literally or by content from the used sources.

Graz, on ....

(Signature)

Kurzfassung

Die Leistungsfähigkeit moderner Kommunikationssysteme hängt stark von den eingesetzten Analog-Digital-Umsetzer (ADU) ab, und um die Flexibilität und Genauigkeit neuartiger Kommunikationstechnologien zu ermöglichen, sind Hochleistungs-Analog-Digital-Wandler erforderlich. In dieser Hinsicht, können zeitlich versetzt operierende ADUs (ZV-ADU) eine angemessene Lösung darstellen. Bei einem ZV-ADU erhöht sich der Datendurchsatz, indem M ADU Kanäle oder Subwandler parallel eingesetzt werden und das Eingangssignal zeitlich versetzt gewandelt wird. Die Leistungsfähigkeit des ZV-ADUs wird durch ungleiche ADU Kanäle stark herabgesetzt. Diese Fehlanpassung der ADU Kanäle verfälscht das Ausgangsspektrum des ZV-ADU, indem unerwünschte Komponenten zusätzlich zu den eigentlichen Signalkomponenten generiert werden. Diese Arbeit befasst sich mit einer im Hintergrund ablaufenden adaptiven Kalibrierung von fehlangepassten Frequenzantworten eines ZV-ADUs. Indem jeder ADU Kanal als lineares zeitinvariantes System modelliert wird, entwickeln wir zeitkontinuierliche, zeitdiskrete und zeitvariante Modelle eines ZV-ADUs. Unter Zuhilfenahme dieser Modelle wird das Verhalten des ZV-ADUs mit fehlangepassten Frequenzantworten charakterisiert. Zu Beginn wird die Fehlanpassung der Frequenzantworten ausschließlich durch Verstärkungs- und Abtastfehlanpassungen modelliert, welche durch Taylor Reihen erster Ordnung angenähert werden. Wir entwerfen anschließend eine blinde im Hintergrund operierende Kalibrierungsstruktur, die einen filtered-X least-mean square (FxLMS) Algorithmus einsetzt um die Verstärkungs- und Abtastfehlanpassungen zu kalibrieren. Neben ihrer Einfachheit und guten Skalierbarkeit funktioniert diese Kalibrierungstechnik auch gut für verschiedene Arten von Eingangssignalen und verbessert die Leistungsfähigkeit des ZV-ADUs beträchtlich. Weiterhin wird eine im Hintergrund operierende digitale und adaptive Technik präsentiert, welche die fehlangepassten Frequenzantworten eines zwei Kanal ZV-ADUs kalibriert. Im Gegensatz zu anderen Kabibrierungstechniken, hängt unsere Kalibrierungstechnik nicht von der Art des Eingangssignals und der Modelle der Kanalfehlanpassung ab. Wir repräsentieren die Fehlanpassung der Frequenzantwort durch eine Reihe von Polynomen von konstanter Ordnung was es uns ermöglicht die Fehlanpassung der Frequenzanworten durch die Koeffizienten der Reihe zu charakterisieren.

Anschließend werden diese Koeffizienten mittels des FxLMS Algorithmus geschätzt, unter dessen Zuhilfenahme das Eingangssignal rekonstruiert wird. Letztendlich wird eine nicht-blinde im Hintergrund operierende Kalibrierungsstruktur präsentiert, die einen weiteren ADU mit niedriger Auflösung als Referenz und ein M-periodisch zeitvariantes Filter verwendet, um die Fehlanpassung der Frequenzantworten zu kalibrieren. Alle genannten digitalen Kalibrierungstechniken ermöglichen es, die durch Fehlanpassung der Frequenzantworten verursachten Leistungseinbußen des ZV-ADUs zu kompensieren.

Abstract

The performance of today's communication systems is highly dependent on the employed analog-to-digital converters (ADCs), and in order to provide more flexibility and precision for the emerging communication technologies, high-performance ADCs are required. In this regard, the time-interleaved operation of an array of ADCs (TI-ADC) can be a reasonable solution. A TI-ADC can increase its throughput by using M channel ADCs or subconverters in parallel and sampling the input signal in a time-interleaved manner. However, the performance of a TI-ADC badly suffers from the mismatches among the channel ADCs. The mismatches among channel ADCs distort the TI-ADC output spectrum by introducing spurious tones besides the actual signal components. This thesis deals with the adaptive background calibration of frequency-response mismatches in a TI-ADC. By modeling each channel ADC as a linear time-invariant system, we develop the continuous-time, discrete-time, and time-varying system models of a TI-ADC. These models help us to characterize the behavior of a TI-ADC in the presence of frequency response mismatches. First we model the channel frequency responses with gain and timing mismatches only which are approximated using a first-order Taylor's series expansion. Consequently, we present a blind calibration structure that uses the filtered-X least-mean square (FxLMS) algorithm to calibrate the gain and timing mismatches. Besides its simplicity and ease of scalability, this calibration technique works well with different types of input signals and significantly improves the performance of a TI-ADC. Next a digital background blind calibration structure for frequency response mismatches in a two-channel TI-ADC is presented. Contrary to the other calibration techniques in the literature, our calibration technique is not dependent on the type of the input signal and the channel mismatch models. We represent the frequency response mismatches by a polynomial series of fixed order that allows us to characterize the mismatch by the coefficients of this series. Later these coefficients are estimated by using the FxLMS algorithm that helps in the reconstruction of the input signal. Finally, a flexible digital background non-blind calibration structure is presented that uses an extra low-resolution ADC as reference and an M-periodic time-varying filter to adaptively calibrate the frequency response mismatches in a TI-ADC. This structure may be used to calibrate any linear frequency response mismatches including gain and timing mismatches. All these digital calibration techniques make it possible to overcome the performance artifacts of frequency response mismatches in a TI-ADC.

Acknowledgement

Several persons supported me during the time of my PhD research. Most important of all is Dr. Christian Vogel, whose wide knowledge and logical way of thinking have been of great value for me. His understanding, encouragement, and personal guidance has led me to this thesis.

I am deeply grateful to my supervisor, Professor Gernot Kubin, for his detailed and constructive comments, and for his important support throughout this work.

My sincere thanks are due, to the second examiner of this thesis, Professor Svante Signell, for his useful comments during the preparation of this thesis.

Thanks to my colleagues at SPSC Lab, and, especially to those with whom I had shared an office, for the interesting discussions, and the fun we had together. I wish to thank Michael Soudan, for writing the 'Kurzfassung' (the German version of the 'Abstract') of this thesis.

I am extremely thankful to Higher Education Commission (HEC), Pakistan, for funding my research.

Special thanks go to my wife Sadia, for her encouragement, and support throughout my research. My children Samra, and Hamza, always provided me excellent company whenever, I was away from research. Above all, I would like to thank my parents for a never-ending support. Last but not least, thanks to my brothers, sisters, relatives, and friends, for providing me moral support throughout the time of my PhD research.

Shahzad Saleem
Graz, December 2010

Contents

1 Introduction **1**

1.1 Time-Interleaved ADCs . . . 1

1.1.1 Working Principle . . . 2

1.1.2 Mismatch Errors . . . 2

1.2 Time-Interleaved ADC Calibration Techniques . . . 4

1.3 Scope of the Work . . . 8

1.4 Outline of the Thesis and Research Contributions . . . 9

2 System Models of a Time-Interleaved ADC **13**

2.1 Introduction . . . 13

2.2 Continuous-Time System Model . . . 15

2.3 Discrete-Time System Model . . . 17

2.4 TI-ADC as an M-Periodic Time-Varying System . . . 22

2.5 Conclusions . . . 23

3 Adaptive Blind Background Calibration of Gain and Timing Mismatches **25**

3.1 Introduction . . . 25

3.2 Taylor's Series Approximated System Model . . . 28

3.3 Adaptive Blind Calibration . . . 30

3.3.1 Main Idea . . . 31

3.3.2 Analysis . . . 33

3.4 Simulation Results . . . 34

3.4.1 Bandlimited White Gaussian Noise Input Signal . . . 35

3.4.2 Bandlimited Multitone Input Signal . . . 37

3.5 Conclusions . . . 38

4 Adaptive Blind Background Calibration of Frequency Response Mismatches Represented by Polynomials **41**

4.1 Introduction . . . 42

4.2 Polynomial Representation of Frequency Response Mismatches . . . 44

4.3 Adaptive Blind Calibration . . . 46

4.3.1 Calibration Principle . . . 46

4.3.2 Calibration Structure . . . 47

4.3.3 Coefficient Adaptation . . . 49

4.3.4 Performance Analysis . . . 50

4.4 Simulation Results . . . 51

4.4.1 Implementation of the Calibration Structure 52
4.4.2 Calibration of Frequency Response Mismatches: White Gaussian Noise Input Signal 54
4.4.3 Calibration of Frequency Response Mismatches: Multitone Input Signal 54
4.4.4 Calibration of Bandwidth Mismatches: Multitone Input Signal . . 57
4.4.5 Calibration of Gain and Timing Mismatches: White Gaussian Noise Input Signal 59
4.5 Conclusions 61

5 Adaptive Non-Blind Background Calibration of Frequency Response Mismatches 63
5.1 Introduction 63
5.2 Cascaded Time-Varying Filters 66
5.3 Adaptive Calibration 67
5.4 Simulation Results 68
5.5 Conclusions 70

6 Summary & Concluding Remarks 73

Bibliography 75

List of Figures

1.1 A time-interleaved ADC with M channels. 2
1.2 Sampling principle of a time-interleaved ADC with M channels. 3
1.3 Continuous-time model of a TI-ADC 4
1.4 TI-ADC mismatch errors 5

2.1 Analog-to-Digital Conversion Model. 14
2.2 Linear model of an ADC 14
2.3 Continuous-time system model of an M-channel TI-ADC 15
2.4 Discrete-time system model of an M-channel TI-ADC 20
2.5 Representing a complex filter as combination of real-valued filters 22
2.6 Time-varying system model of a TI-ADC. 23

3.1 Model of an M-channel TI-ADC with gains and the timing mismatches . 26
3.2 Effect of gain and timing mismatches on the sampling process of a four-channel TI-ADC ($M = 4$). 27
3.3 The first-order Taylor's series approximated discrete-time system model of an M-channel TI-ADC with gain and timing mismatches. 31
3.4 The proposed adaptive blind calibration structure for gain and timing mismatches. 32
3.5 Main idea of blind identification 32
3.6 Power spectrum of the uncalibrated output for the case of a WGN input signal 36
3.7 Power spectrum of the reconstructed input signal 36
3.8 The convergence behavior of the estimated gain mismatch coefficients . . 37
3.9 The convergence behavior of the estimated timing mismatch coefficients . 38
3.10 Power spectrum of the uncalibrated output for the case of a multitone input signal 39
3.11 Power spectrum of the reconstructed output 39
3.12 The convergence behavior of the estimated gain mismatch coefficients . . 40
3.13 The convergence behavior of the estimated timing mismatch coefficients . 40

4.1 Discrete-time system model of a two-channel TI-ADC. 45
4.2 Calibration of frequency response mismatches. 46
4.3 Mismatch band for a two-channel TI-ADC with frequency response mismatches 47

4.4 Calibration structure for polynomial-represented frequency response mismatches . . . 48
4.5 Model of the identification structure illustrating the identification of $\hat{\mathbf{c}}[n]$ coefficients. . . . 50
4.6 Implementation example of the blind calibration structure for $P = 3$. . . . 52
4.7 Magnitude response of the high-pass filter . . . 53
4.8 Power spectrum of the uncalibrated output for a white Gaussian noise (WGN) input signal . . . 55
4.9 Power spectrum of the reconstructed WGN input signal . . . 55
4.10 Convergence behavior of the estimated polynomial coefficients . . . 56
4.11 Power spectrum of the uncalibrated output for a multitone input signal . . . 56
4.12 Power spectrum of the reconstructed multitone input signal . . . 57
4.13 Power spectrum of the output with 5% bandwidth mismatch . . . 58
4.14 Power spectrum of the reconstructed output . . . 59
4.15 Power spectrum of the uncalibrated output with gain and timing mismatches 60
4.16 Power spectrum of the reconstructed output using a 1st order calibration structure . . . 60
4.17 Convergence behavior of the estimated gain mismatch coefficients using the filtered and delayed versions of the LMS algorithm . . . 62
4.18 Convergence behavior of the estimated timing offset coefficients using the filtered and delayed versions of the LMS algorithm . . . 62

5.1 Time-varying system model of a high-resolution TI-ADC with a quantizer Q_H. . . . 65
5.2 A low-resolution ADC with an impulse response $r[n]$ and quantizer Q_L. . . . 65
5.3 Cascade of the two M-periodic time-varying filters . . . 66
5.4 Adaptive non-blind background calibration structure . . . 67
5.5 Power spectrum of the uncompensated output with $Q_H = 16$ bits and $Q_L = 2$ bits . . . 71
5.6 Power spectrum of the compensated output using a compensation filter with 17 taps (once LMS has been converged) . . . 71
5.7 Q_L vs SNR using a compensation filter with 17 taps ($Q_H = 16$ bits). . . . 72
5.8 The filter order L of the compensation filter $g_n[l]$ vs SNR using different values of Q_L. . . . 72

List of Tables

3.1 Simulated gain and timing mismatch values 35

4.1 Simulated bandwidth mismatch values. 58
4.2 Initial and final SNR for different bandwidth mismatch values and for different orders of the calibration structure 58

5.1 Simulated gain mismatches, relative timing and frequency offsets values . 69

List of Abbreviations

A/D	Analog-to-Digital
ADC	Analog-to-digital converter
CMOS	Complementary metal oxide semiconductor
CT	Continuous time
CTFT	Continuous-time Fourier transform
dB	DeciBels
dBc	DeciBels (below) carrier
DFT	Discrete Fourier transform
DNL	Differential nonlinearity
DT	Discrete time
DTFT	Discrete-time Fourier transform
DR	Dynamic-range
ENOB	Effective number of bits
FxLMS	Filtered-X LMS
FIR	Finite impulse response
HFB	Hybrid filter bank
IIR	Infinite impulse response
LS	Least square
LMS	Least-mean square
MUX	Multiplexer
PR	Perfect reconstruction
SFDR	Spurious-free dynamic range
S/H	Sample-and-hold
SINAD	Signal-to-noise and distortion ratio
SNR	Signal-to-noise ratio
TI-ADC	Time-interleaved ADC
WGN	White Gaussian noise
WLS	Weighted least squares

Signals and Variables

Indexes

n	Discrete time index
t	Continuous time index
M	Number of channel ADCs
m	Index of channel ADCs
k	Index of channel ADCs
l	Convolution index

Sampling Frequency

T_s	Sampling time period
f_s	Sampling frequency

Input Signals

$x(t)$	Analog input signal
$X(\ )$	Input signal in the Fourier domain
$x[n]$	Digital input signal
$\bar{x}[n]$	Digital reference input signal
$\bar{X}(\ )$	Reference input signal in the Fourier Domain
$\hat{x}[n]$	Reconstructed digital input signal
$x_p[n]$	pth time modulated and differentiated reference input signal $\bar{x}[n]$
$\mathbf{x}_d[n]$	Modulated and differentiated reference input signal vector
$\mathbf{x}_d^f[n]$	High-pass filtered vector $\mathbf{x}_d[n]$

Output Signals

$Y(\ )$	Output Signal in the Fourier domain
$y[n]$	Digital output signal
$\hat{y}[n]$	Quantized output signal
$y_c[n]$	Compensated output signal
$e[n]$	Digital error signal

$x_r[n]$	Digital output of a low-resolution ADC
$\hat{d}[n]$	Quantized output of a low-resolution ADC
$y_p[n]$	pth time modulated and differentiated digital output signal $y[n]$
$\mathbf{y}_d[n]$	Modulated and differentiated output signal vector
$\mathbf{y}_d^f[n]$	High-pass filtered vector $\mathbf{y}_d[n]$
$\hat{e}[n]$	Estimated digital error signal
$e_p[n]$	pth time modulated and differentiated error signal $e[n]$
$\mathbf{e}_d[n]$	Modulated and differentiated error signal vector
$\mathbf{e}_d^f[n]$	High-pass filtered vector $\mathbf{e}_d[n]$

Mismatch Variables

r_m	Timing Mismatch
g_m or α_m	Gain Mismatch
o_m	Offset Mismatch
Δ	Relative frequency offset or bandwidth mismatch
R_k	Timing mismatch coefficients
G_k	Gain mismatch coefficients
$\mathbf{c}_r$	Timing mismatch coefficients vector
$\mathbf{c}_g$	Gain mismatch coefficients vector
$\mathbf{m}[n]$	Modulation vector
$\hat{\mathbf{c}}_r[n]$	Estimated timing mismatch coefficients vector
$\hat{\mathbf{c}}_g[n]$	Estimated gain mismatch coefficients vector
$\mathbf{x}_g[n]$	Modulated signal vector
$\mathbf{x}_r[n]$	Modulated and differentiated signal vector
$\breve{c}_p$	pth coefficient of the polynomial series
$\mathbf{c}$	Polynomial series coefficients vector
$\hat{c}_p[n]$	Estimated pth coefficient of the polynomial series
$\hat{\mathbf{c}}[n]$	Estimated polynomial series coefficients vector

Symbols and Operators

General Notation

$[.]^T$	Transpose
$\delta(\ )$	Dirac delta distribution
$E\{\ \}$	Expectation operator
Q	Quantizer
Q_H	Quantizer with high resolution
Q_L	Quantizer with low resolution
σ_x^2	Variance of the input signal $x[n]$

Correlation

$\mathbf{R}$	Autocorrelation matrix
$\mathbf{p}$	Cross correlation vector

Frequency Symbols

Ω	Analog frequency
ω	Discrete frequency
Ω_s	Analog sampling frequency
Ω_c	3 dB cutoff frequency

Adaptation Symbols

ε	Adaptation error
μ	Step-size parameter
μ_g	Step-size parameter for gain mismatch
μ_r	Step-size parameter for timing mismatch

Transfer Functions

$H_d(e^{j\omega})$	Discrete-time frequency response of a differentiator
$D_p(e^{j\omega})$	Discrete-time P-th order differentiator
$\hat{H}_m(j\Omega)$	Continuous-time channel frequency response

$H_m(e^{j\omega})$	Discrete-time channel frequency response
$\breve{H}_k(e^{j\omega})$	Summation over $H_m(e^{j\omega})$
$\breve{H}_0(e^{j\omega})$	Average channel frequency response
$\breve{Q}_k(e^{j\omega})$	Normalized channel frequency response mismatch

Impulse Responses

$h_d[n]$	Inverse DTFT of $H_d(e^{j\omega})$
$d_p[n]$	Inverse DTFT of $D_p(e^{j\omega})$
$r[n]$	Impulse response of a low-resolution ADC
$f[n]$	Impulse response of a high-pass filter
$h_n[l]$ or $g_n[l]$ or $f_n[l]$	Impulse response of a time-varying filter
$\hat{h}_m[n]$	Inverse DTFT of $\hat{H}_m(j\Omega)$
$h_m[n]$	Inverse DTFT of $H_m(e^{j\omega})$
$\breve{h}_k[n]$	Inverse DTFT of $\breve{H}_k(e^{j\omega})$
$\breve{h}_0[n]$	Inverse DTFT of $\breve{H}_0(e^{j\omega})$
$\breve{q}_k[n]$	Inverse DTFT of $\breve{Q}_k(e^{j\omega})$
$\hat{q}_k[n]$	Estimated $\breve{q}_k[n]$

1 Introduction

Analog-to-digital converters (ADCs) are critical components in many communication systems [1]. The current trend is to move more and more of the functionality of a communication system into the digital domain in order to provide an increased flexibility and reduced cost [2, 3]. To accomplish this, the requirements on the data converters increase both in terms of higher accuracy and larger bandwidth. One way to increase the bandwidth of an ADC is to use several ADCs in parallel and to sample data in a time-interleaved fashion [4].

Unfortunately, the performance of the interleaved architecture suffers from mismatches among the subconverters[1, 5]. This is mainly caused by the difference in the characteristics of the components used in the ADCs. These mismatches are often expressed as relative errors measured with respect to some nominal reference channel. In recent years, due to the availability of several calibration techniques in the analog and digital domains, it has become possible to improve the performance of a time-interleaved ADC (TI-ADC) [6–18].

This chapter gives an overview of the operation of time-interleaved ADCs and of the mismatches which occur in the sampling process. It reviews previous blind and non-blind calibration methods and outlines the contributions of this thesis.

1.1 Time-Interleaved ADCs

In this section the working principle of a TI-ADC is introduced. We further discuss the performance degradation of the interleaved architecture due to the mismatches among the sub-ADCs. This may be caused due to the difference in the characteristics of the different components used in ADCs. By knowing the nature of the mismatches it is possible to design calibration structures to reduce the effects of these mismatches.

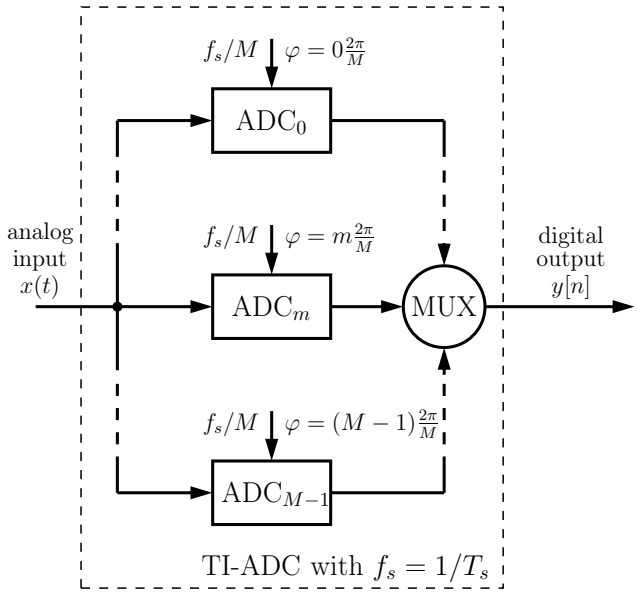

Figure 1.1: *A time-interleaved ADC with M channels.*

1.1.1 Working Principle

A time-interleaved ADC operates at a higher sampling rate by utilizing an array of multiple ADCs with lower sampling rates [4, 19]. The bandlimited analog input signal $x(t)$ is processed by the sub-ADCs in a time-interleaved manner to produce the digital output $y[n]$. As shown in Fig. 1.1, the conversion rate in each individual ADC is reduced to f_s/M where the phase of the clock for the mth channel ADC is given by $\varphi = m\frac{2\pi}{M}$, while the overall sampling rate is kept at f_s, where M is the number of ADCs that are used in parallel.

In terms of the timing of a TI-ADC, a sample is taken by another sub-ADC at each time step and a digital output is produced. Hence each channel ADC has a sampling period of MT_s and the overall time-interleaved system has a period of T_s as illustrated by Fig. 1.2. A multiplexer (MUX) merges the samples from the sub-ADCs into a single data stream. It should be noticed, however, that the sampling unit in each sub-ADC has to deal with the entire analog bandwidth of the input signal, otherwise the sampled signal would be distorted.

1.1.2 Mismatch Errors

As mentioned before, the overall performance of a TI-ADC suffers from mismatches among the sub-ADCs such as offset, gain, timing-skew, and bandwidth mismatches [20].

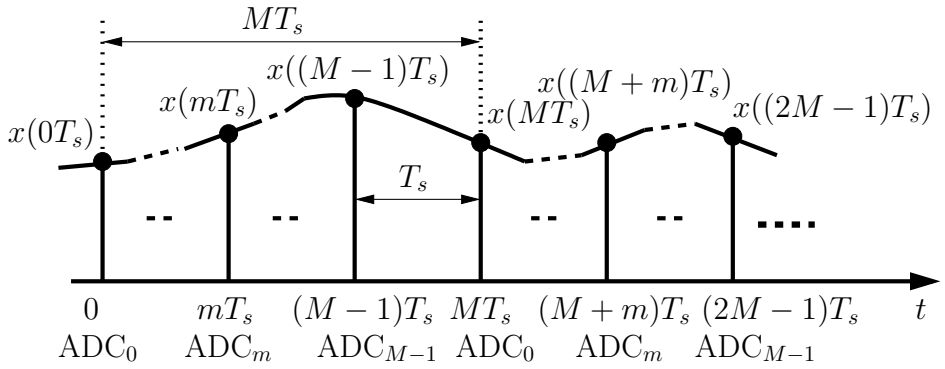

Figure 1.2: *Sampling principle of a time-interleaved ADC with M channels.*

The presence of mismatches among the sub-ADCs distort the TI-ADC output spectrum by introducing spurious tones beside the actual signal components. As shown in Fig. 1.3 it is reasonable to model each channel ADC inside a TI-ADC by a linear time-invariant (LTI) system with an analog frequency response $\hat{H}_m(j\Omega)$ followed by a sampler, where Ω is the analog frequency and $m = 0, 1, \ldots, M-1$ [21, Ch 4]. The frequency responses include all linear characteristics such as gain, time offsets, and bandwidth. If the frequency responses $\hat{H}_m(j\Omega)$ differ among the channel ADCs, then frequency response mismatches arise in a TI-ADC. Let us consider a two-channel TI-ADC ($M = 2$)with channel frequency responses

$$\hat{H}_m(j\Omega) = \frac{g_m}{1 + j\frac{\Omega}{(1+\Delta_m)\Omega_c}} e^{j\Omega T r_m} \tag{1.1}$$

where Ω_c is the 3-dB cutoff frequency of the first order response, g_m are the gain mismatches, Δ_m are the relative frequency offsets from Ω_c, and r_m are the relative timing offsets from the ideal sampling instants. The input signal $x(t)$ is a single sinusoidal tone with unit amplitude at some frequency $0.1088\Omega_s/2$, where $\Omega_s/2 = \pi/T_s$ is half sampling frequency as shown in Fig. 1.4(a). In addition to this tone, the frequency response mismatch introduces a second tone in the TI-ADC output at frequency $0.8912\Omega_s/2$ as shown in Fig. 1.4(b). This leads to degradation in the performance of a TI-ADC that can be characterized by different measures such as signal-to-noise and distortion ratio (SINAD), and spurious-free dynamic range (SFDR) [22].

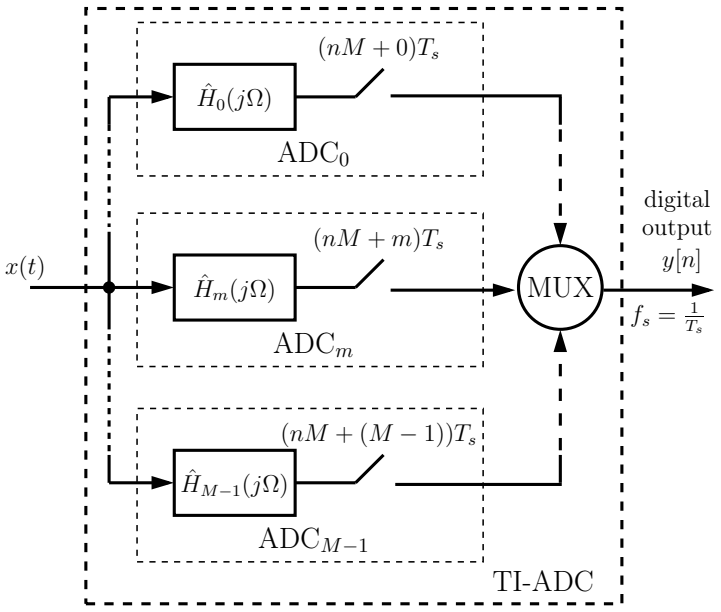

Figure 1.3: *Model of a TI-ADC with M channels where each channel is represented by an LTI system with analog frequency response $\hat{H}_m(j\Omega)$ with $m = 0, 1, \ldots, M-1$ followed by a sampler.*

1.2 Time-Interleaved ADC Calibration Techniques

As discussed in the last section the mismatches reduce the performance of a TI-ADC. One solution to avoid mismatches is to use a single ADC with a higher sampling rate, but this is costly and unrealizable. Hence there is need for calibration techniques that are able to identify and correct the mismatches. Some techniques perform the calibration in the foreground such that they need special calibration phases to inject a test signal during the operation of an ADC, thus causing system interruptions. Alternatively there are techniques that do not need any test signal and thus perform the calibration in the background while the ADC is performing its normal operation. Furthermore, we can categorize the calibration process as non-blind or blind. The non-blind calibration requires knowledge about the input signal while the blind calibration works without knowledge of the input signal.

Formally every calibration technique consists of two phases, i.e., identification and reconstruction. The identification phase estimates the mismatches using either non-adaptive or adaptive algorithms [23]. An adaptive algorithm self-adjusts itself according

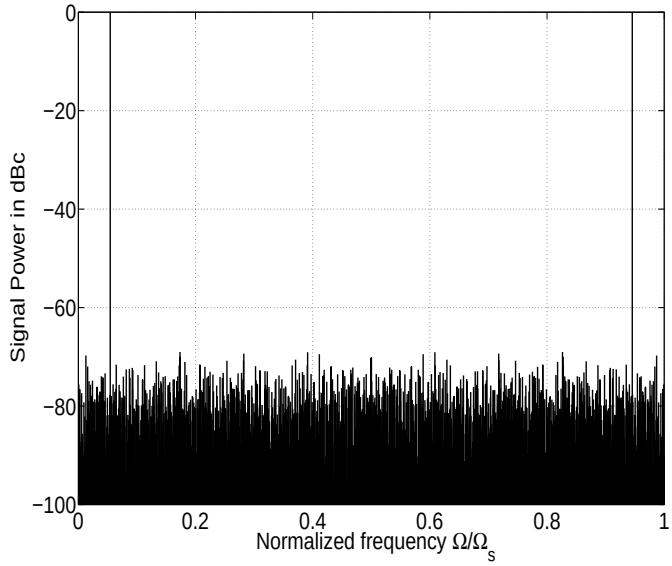

(a) Output of a two-channel TI-ADC without mismatches.

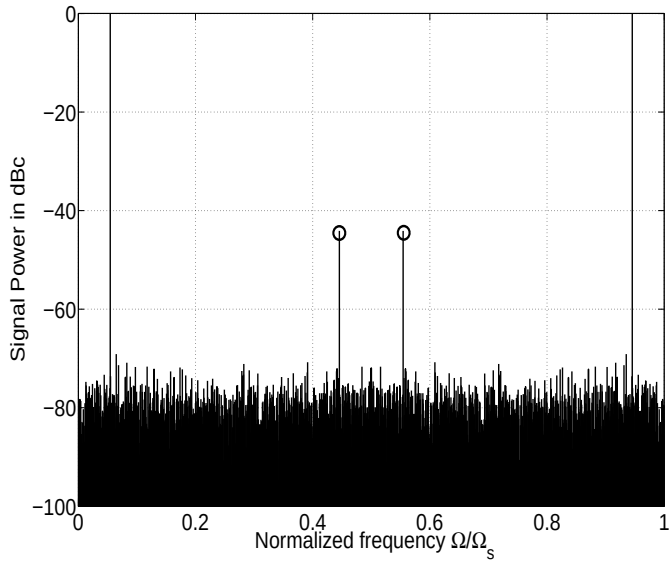

(b) Output of a two-channel TI-ADC with frequency response mismatches.

Figure 1.4: *These figures show the typical output spectra of a two-channel time-interleaved ADC without mismatches Fig. 1.4(a) and with frequency response mismatches Fig. 1.4(b), where signal power is shown along y-axis in deciBels (below) carrier (dBc). For both figures we have used a sinusoidal input signal with a frequency of* $0.1088\Omega_s/2$. *Fig. 1.4(a) looks like the output of a conventional ADC, whereas Fig. 1.4(b) has an additional spurious tone at* $0.8912\Omega_s/2$ *(denoted with circles), which is caused by the frequency response mismatch.*

to an optimization criterion to get the optimum estimate of the mismatches. By contrast, a non-adaptive algorithm finds the mismatch estimates in a static way by explicitly solving some equations. The correct estimation of the mismatches generates the reconstructed input signal. In other words the performance of the reconstruction process is highly dependent on the accuracy of the estimated mismatch values.

Since the invention of time-interleaved converter arrays by Black [4, 19], the analysis and calibration of mismatch errors in TI-ADCs have attracted many researchers during the last three decades. The mismatch analysis techniques have addressed the effects of offset, gain, timing, and bandwidth mismatches beside quantization effects on the performance of TI-ADCs [20, 24–29]. Beside that many calibration techniques for offset, gain, and timing mismatches in analog and digital domains have been presented [6–13, 30–47, 47–55].

The techniques addressing only the calibration of offset and gain mismatches include [6, 7, 47]. In [6] a digital background calibration scheme to overcome the effects of offset and gain mismatches was presented. Background calibration was performed by adding a calibration signal to the ADC input and processing both simultaneously. An analog blind calibration technique using adaptive signal processing, an extra channel, and mixed-signal integrators to calibrate the offsets and gains of time-interleaved channels in a 10-b 40-MSample/s pipelined ADC was presented in [7]. With monolithic background calibration, a peak SNDR of 58 dB, and power dissipation of 650 mW was achieved in 1 μm CMOS. In [47] a software method based on the fast Fourier transform (FFT) for offset and gain error compensation was presented.

The problem of nonuniform sampling that leads to the timing mismatches in a TI-ADC and the reconstruction of nonuniformly sampled signals has been investigated in [30–36, 38–42, 48, 52, 53]. Jenq was the first who addressed this problem [30–33]. He developed a unified representation of a TI-ADC output for the case of nonuniform sampling. Marvasti et al. have investigated the theoretical aspects of nonuniform sampling and have proposed iterative methods for recovering one and multidimensional signals from their nonuniform samples in [34–36]. A discrete-time filter bank implementation for the reconstruction of a periodically nonuniform sampled signal was presented in [48]. The reconstruction filters were evaluated based on a method approximating the perfect reconstruction (PR) condition that gave an uniformly sampled output with negligible distortions and transfer of alias components. Johansson et al. have investigated foreground reconstruction of nonuniformly sampled signals using digital fractional-delay and polynomial impulse response time-varying finite-impulse response (FIR) filters in [38–42]. They have used a multirate filter bank [56] based reconstruction system. Furthermore

they have used a least-squares method to get an analytic solution for the synthesis filters in a multirate filter-bank. A novel method for the reconstruction of two-periodic and non-periodic nonuniformly sampled signals has been presented in [52, 53]. The authors have proposed a differentiator-multiplier cascade based reconstruction structure that by utilizing the values of timing deviations can reconstruct a replica of the error signal due to the nonuniform sampling. This error signal is later subtracted from the nonuniformly sampled output to get the reconstructed input signal. By far this is the simplest of the available reconstruction schemes since it only involves fixed filters like differentiators and a few multipliers. We have used a similar reconstruction strategy in our blind background calibration techniques for gain, timing, and frequency response mismatches that will be presented in chapters 3 and 4 of this thesis.

The techniques that jointly address the estimation and compensation of offset, gain, and timing mismatches have been presented in [9–13, 43–46, 49–51, 54, 55, 57]. A robust sampling time offset estimation algorithm to perfectly reconstruct the digital spectrum of a TI-ADC from nonuniformly sampled signals was presented in [57]. Another digital background calibration technique was proposed in [8, 37] to minimize the timing-error effects in a TI-ADC. This technique was based on the digital interpolation, which estimated the correct output values from the output samples that suffer from timing errors. Jamal et al. designed a two-channel time-interleaved ADC with digital background calibration for the offset, gain, and timing mismatches [9, 43]. Elbornsson et al. have investigated blind adaptive equalization of offset, gain, and timing mismatches in a TI-ADC with measurement results in [10, 44–46]. Seo et al. have investigated blind calibration of gain, and timing mismatches in [11, 49] using a multirate filter-bank structure. Vogel et al. have worked on modeling, identification and compensation of channel mismatch errors in TI-ADCs [58–60]. They have worked not only on the blind identification and compensation of timing mismatches [50, 51] but on the compensation of nonlinearity mismatches as well [61]. Huang et al. have investigated the blind calibration of gain and timing mismatches in TI-ADCs [12, 54, 62]. Another blind calibration technique for timing mismatches have been proposed in [13, 55]. The authors have calculated both the least squares and LMS solutions for the calibration structure. Since the focus of this thesis is to develop adaptive calibration techniques only, hence if we look at the existing adaptive calibration techniques for offset, gain, and timing mismatches, e.g., [9–13, 43, 49, 54, 55], then most of these techniques are limited to two-channel TI-ADCs only [9, 11–13, 43, 49, 55], which simplifies the identification problem. Only the method in [54] addresses the calibration of timing mismatches in a four-channel TI-ADC. The authors of [10] have equalized the offset, gain, and timing mismatches for an M-channel

TI-ADC. However their method has high complexity. In chapter 3 of this thesis we introduce a different adaptive blind background technique to calibrate the gain, and timing mismatches for an M-channel TI-ADC. This structure has limited complexity and gives a significant improvement in the performance of a TI-ADC.

During the last five years the main emphasis has been on the calibration of frequency response mismatches since this is a kind of generalized mismatch calibration that can lead to further improvements in the performance of a TI-ADC [63]. In recent years several techniques addressing the calibration of bandwidth mismatches [64–66] and frequency response mismatches have been published [63, 67–75]. Most of these methods are neither adaptive nor blind [67–72, 75]. The other methods either require special input signals [63, 74] or specific forms of the channel frequency responses [73]. In chapters 4 and 5 of this thesis we present the fully blind and non-blind methods respectively to adaptively calibrate the frequency response mismatches in a TI-ADC. Both of these methods are able to work with different types of mismatch models and input signals.

1.3 Scope of the Work

The main objective of this work is to develop calibration methods in the digital domain that can calibrate the frequency response mismatches in a TI-ADC. Since a TI-ADC is also characterized as a time-varying system hence one property of the methods should be their ability to track these time-variations which is possible if we use adaptive techniques that are simple to implement and provide robust performance [23]. A second property is the ability to work in the background, i.e., without interrupting the normal conversion process. Another property is to perform the background calibration in such a way that avoids any complex filter design methods.

The calibration methods can be roughly divided in blind and non blind methods. In order to design such methods, we have developed system models of a TI-ADC both in continuous time, and discrete time. On the one hand, these models help to describe the mismatch behavior by explicitly dividing its output into a reference signal that is less affected by the mismatches and an error signal that is due to the mismatches. One part of our research was to approximate the error signal using the first-order Taylor's series (for the calibration of gain and timing mismatches) and a P-th order polynomial (for the calibration of frequency response mismatches) such that the coefficients of the polynomial implicitly carry the information about mismatches. Hence we have developed the blind background calibration methods that adaptively estimate these coefficients in order to produce an estimated error signal that is subtracted from the TI-ADC output

to give us the reconstructed input signal. On the other hand, system models can also characterize the TI-ADC output as that of an M-periodic time-varying system that exhibits a different behavior at each sampling instant. Therefore, another part of our research was to use an M-periodic time-varying filter to calibrate frequency response mismatches in a high-resolution TI-ADC. However in order to find the coefficient sets of the time-varying filter in an adaptive way we need a reference signal that was obtained by using an additional low-resolution ADC. Such an ADC does not significantly increase the power consumption of a high-resolution TI-ADC. In this way, we have also discovered a non-blind method that can suppress the time-varying nature of a TI-ADC to produce the frequency response mismatch compensated output. A more detailed conclusion and a further discussion of the work is given in chapter 6.

1.4 Outline of the Thesis and Research Contributions

In this thesis we present the adaptive background blind and non-blind calibration techniques for frequency response mismatches in a TI-ADC. However we do not focus on some specific technology of ADCs [76, 77, Ch 3]. In the following we present a brief outline of the thesis.

Chapter 2: System Models of a Time-Interleaved ADC

In chapter 2, we present the continuous-time, discrete-time, and M-periodic time varying system models of an M-channel TI-ADC. These models provide a systematic way to represent the output of a TI-ADC.

Chapter 3: Adaptive Blind Background Calibration of Gain and Timing Mismatches

In chapter 3 we discuss the blind calibration of gain and timing mismatches in an M-channel TI-ADC. Gain and timing mismatches are special cases of frequency response mismatches that effect the input signal amplitude and frequency respectively. We perform blind identification of gain and timing mismatches based on a first-order Taylor's series [78] approximation of the mismatches. The adaptive identification structure uses only fixed filters that include one differentiator, $2(M-1)$ modulators, $2(M-1)$ time-varying multipliers, and a single high-pass filter, where M is number of channel ADCs. This efficient implementation of the blind identification structure is later exploited in chapter 4 to identify and compensate polynomial-represented frequency response mismatches. The publications to this chapter are

- Shahzad Saleem and Christian Vogel, "LMS-based Identification and Compensation of Timing Mismatches in a Two-Channel Time-Interleaved Analog-to-Digital Converter", Proceedings of the IEEE Norchip Conference 2007, Aalborg, Denmark, November 2007 [16].
- Shahzad Saleem, "Adaptive Blind Calibration Techniques for Gain-Timing and Generalized Mismatch Models in Time-Interleaved Analog-to-Digital Converters", Technical Report, Signal Processing and Speech Communication Laboratory, Graz University of Technology, Austria [79].
- Christian Vogel, Shahzad Saleem and Stefan Mendel, "Adaptive Blind Compensation of Gain and Timing Mismatches in M-Channel Time-Interleaved ADCs", Proceedings of the 15th IEEE International Conference on Electronics, Circuits and Systems (ICECS 2008), St. Julians, Malta, pp. 49-52, September 2008 [17].
- Shahzad Saleem, "A Comparative Analysis of Adaptive Blind Calibration Techniques for Time-Interleaved ADCs", Proceedings of the 16th Austrian Workshop on MicroElectronics (Austrochip 2008), Linz, Austria, pp. 33-37, October 2008 [80]
- Shahzad Saleem and Christian Vogel, "On Blind Identification of Gain and Timing Mismatches in Time-Interleaved Analog-to-Digital Converters", Proceedings of the 33rd International Conference on Telecommunications and Signal Processing, Baden, Austria, pp. 151-155, August 2010 [14]

Chapter 4: Adaptive Blind Background Calibration of Frequency Response Mismatches Represented by Polynomials

Chapter 4 introduces an adaptive calibration structure for the blind calibration of frequency response mismatches in a two-channel TI-ADC. By representing frequency response mismatches as polynomial series of fixed order, we can exploit slight oversampling, to estimate the coefficients of the polynomials by using the filtered-X LMS (FxLMS) algorithm [81, 82]. Utilizing the coefficients in the adaptive structure, we can compensate frequency response mismatches including gain, timing, and bandwidth mismatches. We develop an analytical framework for the calibration structure and analyze its performance. The publication to this chapter includes

- Shahzad Saleem and Christian Vogel, "Adaptive Blind Background Calibration of Polynomial-Represented Frequency Response Mismatches in a Two-Channel Time-Interleaved ADC", IEEE Transactions on Circuits and Systems I: Regular Papers, Accepted for Publication, 2010 [15]

Chapter 5: Adaptive Non-Blind Background Calibration of Frequency Response Mismatches

In chapter 5 we present a structure comprising an M-channel high resolution TI-ADC and an additional low-resolution ADC. The output of the low-resolution ADC acts as reference to adaptively estimate the coefficient sets of an M-periodic time-varying FIR filter that can calibrate the frequency response mismatches in a TI-ADC. The publication to this chapter is

- Shahzad Saleem, and Christian Vogel, "Adaptive Compensation of Frequency Response Mismatches in High-Resolution Time-Interleaved ADCs using a Low Resolution ADC and a Time-Varying Filter", Proceedings of IEEE International Symposium on Circuits and Systems (ISCAS 2010), Paris, France, pp. 561-564, May-June 2010 [18]

2

System Models of a Time-Interleaved ADC

In this chapter[1], we present the continuous-time, discrete-time, and M-periodic time varying system models of an M-channel TI-ADC. These models provide a systematic way to represent the output of a TI-ADC. By choosing an appropriate form for the frequency responses of the channel ADCs with mismatches, we can decompose the TI-ADC output into a reference signal without mismatches and an error signal due to the mismatches. This decomposition allows to design the calibration structure based on the analytical form of the error signal as discussed in chapter 1. Another possibility is to represent an M-channel TI-ADC as an M-periodic time-varying system where at each sampling instant we get a different response of the TI-ADC system.

In Sec. 2.1 we introduce time-interleaved ADC modeling with mismatches. Sec. 2.2 demonstrates the continuous-time system model of an M-channel TI-ADC and in Sec. 2.3 we develop an alternate representation of the system model, i.e., the discrete-time system model. Finally Sec. 2.4 discusses the M-periodic time-varying system model of a TI-ADC.

2.1 Introduction

In a signal processing system, an ADC converts an analog signal into a digital signal, i.e., a sequence of finite-precision or quantized samples [21]. This task is accomplished by the system shown in Fig. 2.1. The A/D conversion is started and completed every T_s seconds under the control of a clock. However, this conversion is not instantaneous and because of this reason the input value must necessarily be held constant during the time that the converter performs a conversion. This task is accomplished by a sample-and-hold (S/H) circuit that stores the input sample value at the sampling instant and holds it for the

[1]Parts of this chapter have been published in [15, 18, 71]

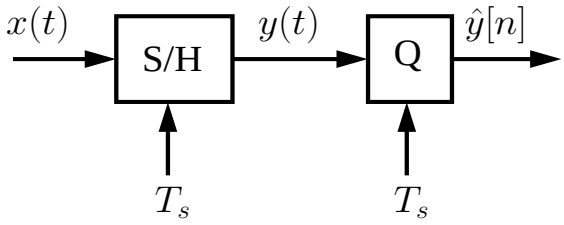

Figure 2.1: *Analog-to-Digital Conversion Model.*

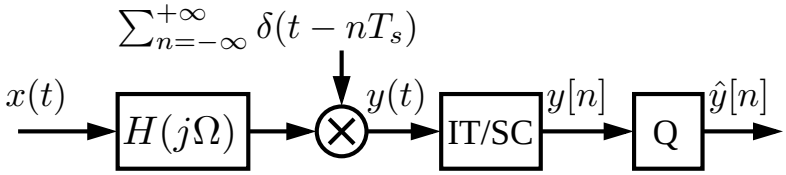

Figure 2.2: *Linear model of an ADC with a LTI frequency response $H(j\Omega)$ followed by the multiplication with an impulse train $\sum_{n=-\infty}^{+\infty} \delta(t - nT_s)$ that yields the sampled signal $y(t)$ which is passed on to an impulse-train to sequence converter (IT/SC) to result in the output sequence $y[n]$. Afterwards a quantizer Q produces the quantized samples $\hat{y}[n]$.*

next sampling time [21]. The output of the S/H is later quantized by a quantizer to produce the digital output $\hat{y}[n]$.

The model shown in Fig. 2.1 can be replaced by a linear model of an ADC as shown in Fig. 2.2. The model assumes that the S/H can be represented by a filter $H(j\Omega)$ followed by the multiplication with an impulse-train $\sum_{n=-\infty}^{+\infty} \delta(t - nT_s)$ where $\delta(t)$ is the Dirac delta distribution. Although this is not fully true in practice, it was shown in [64, 66], that even a model which considers the transient effects of a S/H can be transformed with some modifications of the frequency responses into the model shown in Fig. 2.2. The multiplication with the impulse-train produces the analog output $y(t)$ which is passed on to an impulse-train to sequence converter (IT/SC) to produce the output sequence $y[n]$. Later the sequence $y[n]$ is passed through a quantizer to produce the quantized samples $\hat{y}[n]$.

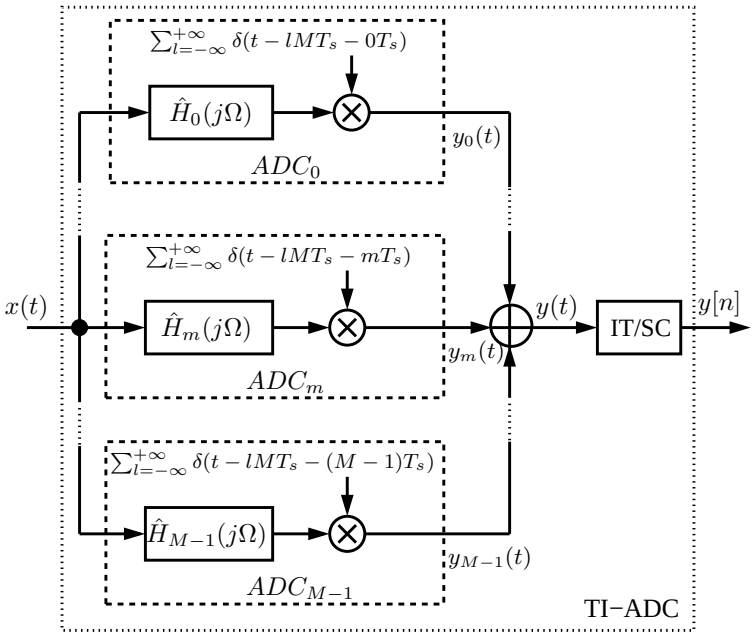

Figure 2.3: *Continuous-time system model of an M-channel TI-ADC [71]. The sampled sequences $y_m(t)$ for $m = 0, 1, \ldots, M-1$, are added and passed on to IT/SC to produce the output sequence $y[n]$.*

2.2 Continuous-Time System Model

In this Section, we present the continuous-time system model of an M-channel TI-ADC as shown in Fig. 2.3 [71]. This model is based on the linear model of an ADC as shown in Fig. 2.2 where the frequency response of the mth channel ADC is represented by $\hat{H}_m(j\Omega)$. The impulse-train contains the time-shift mT_s that accounts for the time-interleaving and MT_s denotes the sampling period of each channel ADC. The sampled signals $y_m(t)$ are merged into the output stream $y(t)$, which becomes $y[n]$ after passing through IT/SC.

From Fig. 2.3, we can write the output of the mth channel ADC as

$$y_m(t) = \sum_{l=-\infty}^{+\infty} \Big(\hat{h}_m(t) * x(t)\Big)\delta(t - lMT_s - mT_s), \tag{2.1}$$

where * denotes convolution operation and

$$\hat{h}_m(t) = \frac{1}{2\pi}\int_{-\infty}^{+\infty} \hat{H}_m(j\Omega)e^{j\Omega t}d\Omega \tag{2.2}$$

is the inverse continuous-time Fourier transform (CTFT) of $\hat{H}_m(j\Omega)$.

Adding the outputs of the M channels gives the sampled output of the TI-ADC

$$y(t) = \sum_{m=0}^{M-1} y_m(t). \tag{2.3}$$

By replacing $y_m(t)$ with (2.1) and rearranging, we obtain [5]

$$y(t) = \sum_{m=0}^{M-1} \Big(\underbrace{\hat{h}_m(t) * x(t)}_{\tilde{x}_m(t)} \Big) \underbrace{\sum_{l=-\infty}^{+\infty} \delta(t - lMT_s)}_{s(t)} * \delta(t - mT_s). \tag{2.4}$$

From (2.4), we see that $y(t)$ is the product of $\tilde{x}_m(t)$ and $s(t)$, therefore the CTFT of $Y(j\Omega)$ is the convolution of the CTFTs of $\tilde{x}_m(t)$ and $s(t)$, i.e., [21, Ch 2]

$$Y(j\Omega) = \sum_{m=0}^{M-1} \frac{1}{2\pi} \Big(\tilde{X}_m(j\Omega) * S(j\Omega) \cdot e^{-j\Omega m T_s} \Big). \tag{2.5}$$

The CTFT $S(j\Omega)$ of the periodic impulse train with period MT_s is given by [83, Ch 4]

$$S(j\Omega) = \frac{2\pi}{MT_s} \sum_{q=-\infty}^{+\infty} \delta\left(\Omega - q\frac{2\pi}{MT_s}\right), \tag{2.6}$$

and the CTFT $\tilde{X}_m(j\Omega)$ of $\tilde{x}_m(t)$ using the convolution theorem can be written as

$$\tilde{X}_m(j\Omega) = \hat{H}_m(j\Omega) X(j\Omega). \tag{2.7}$$

Substituting (2.6)-(2.7) in (2.5) and manipulating gives

$$Y(j\Omega) = \frac{1}{T_s} \sum_{q=-\infty}^{+\infty} \breve{H}_q\left(j\left(\Omega - q\frac{2\pi}{MT_s}\right)\right) X\left(j\left(\Omega - q\frac{2\pi}{MT_s}\right)\right), \tag{2.8}$$

with

$$\breve{H}_q(j\Omega) = \frac{1}{M} \sum_{m=0}^{M-1} \hat{H}_m(j\Omega) e^{-jqm\frac{2\pi}{M}}. \tag{2.9}$$

Equation (2.8) gives the CTFT representation of the output $y[n]$ of an M-channel TI-ADC. If the frequency responses $\hat{H}_m(j\Omega)$ differ from each other then we experience frequency response mismatches in a TI-ADC that distort its output spectrum by introducing spurious images beside the input signal. In order to get a representation for the error introduced by mismatches, we will use (2.8) as starting point to develop a discrete-time system model, where we can explicitly divide the TI-ADC output into a reference signal without mismatches and an error signal due to mismatches.

2.3 Discrete-Time System Model

In this section, we develop the discrete-time representation $Y(e^{j\omega})$ for the output $Y(j\Omega)$ in (2.8). However, we first exploit a useful relation between the analog frequency Ω and the discrete frequency ω.

In the time-domain we can represent the process of sampling through the modulation of a continuous-time signal with a periodic impulse-train $\sum_{n=-\infty}^{+\infty} \delta(t-nTs)$. The sampled signal can be expressed as [21]

$$x_s(t) = \sum_{n=-\infty}^{+\infty} x(t)\delta(t - nT_s). \tag{2.10}$$

The CTFT of (2.10) is

$$X_s(j\Omega) = \sum_{n=-\infty}^{+\infty} x(nT_s)e^{-j\Omega T_s n}. \tag{2.11}$$

Since a sequence of samples $x[n]$ is obtained from a continuous-time signal $x(t)$ through sampling with period T_s using the relation

$$x[n] = x(nT_s). \quad -\infty < n < \infty. \tag{2.12}$$

The discrete-time Fourier transform (DTFT) of the sequence $x[n]$ is given by

$$X(e^{j\omega}) = \sum_{n=-\infty}^{+\infty} x[n]e^{-j\omega n}. \tag{2.13}$$

If we compare (2.13) with (2.11), then it follows that

$$X_s(j\Omega) = X(e^{j\omega})|_{\omega=\Omega T_s} = X(e^{j\Omega T_s}). \tag{2.14}$$

By developing the term $\delta(t - nT_s)$ into a Fourier series, we get another representation for the CTFT of (2.10) which is

$$X_s(j\Omega) = X(e^{j\Omega T_s}) = \frac{1}{T_s}\sum_{n=-\infty}^{+\infty} X(j(\Omega - n\Omega_s)). \tag{2.15}$$

The equivalent DTFT representation of (2.15) while using (2.14) can be written as

$$X(e^{j\omega}) = \frac{1}{T_s}\sum_{n=-\infty}^{+\infty} X\left(j\left(\frac{\omega}{T_s} - n\frac{2\pi}{T_s}\right)\right). \tag{2.16}$$

To get $Y(e^{j\omega})$, we can express the summation index q in (2.8) as

$$q = k + nM, \quad -\infty < n < \infty, \quad 0 \leq k \leq M-1. \tag{2.17}$$

Substituting (2.17) in (2.8) and rearranging gives the DTFT representation of $Y(e^{j\omega})$ as

$$Y(e^{j\omega}) = \sum_{k=0}^{M-1} \left[\frac{1}{T_s} \sum_{n=-\infty}^{+\infty} \breve{H}_k \left(j \left(\frac{\omega - k\frac{2\pi}{M}}{T_s} - n\frac{2\pi}{T_s} \right) \right) X \left(j \left(\frac{\omega - k\frac{2\pi}{M}}{T_s} - n\frac{2\pi}{T_s} \right) \right) \right] \tag{2.18}$$

If we assume that the input signal $x(t)$ is bandlimited, i.e., its CTFT $X(j\Omega)$ satisfies

$$X(j\Omega) = 0, \quad |\Omega| \geq B, \quad BT_s \leq \pi, \tag{2.19}$$

where B is the signal bandwidth then using (2.16) we can finally express (2.18) in discrete time as

$$Y(e^{j\omega}) = \sum_{k=0}^{M-1} \breve{H}_k(e^{j(\omega - k\frac{2\pi}{M})}) X(e^{j(\omega - k\frac{2\pi}{M})}), \tag{2.20}$$

where

$$\breve{H}_k(e^{j\omega}) = \frac{1}{M} \sum_{m=0}^{M-1} H_m(e^{j\omega}) e^{-jk\frac{2\pi}{M}m}, \tag{2.21}$$

and the discrete-time channel frequency responses $H_m(e^{j\omega})$ are the 2π-periodic extension of the analog channel frequency responses $\hat{H}_m(j\Omega)$, i.e.,

$$H_m(e^{j\omega}) = \hat{H}_m(j\frac{\omega}{T}) \text{ for } -\pi \leq \omega < \pi. \tag{2.22}$$

In order to get an expression for the error signal due to the frequency response mismatches, we decompose (2.20) as

$$Y(e^{j\omega}) = \bar{X}(e^{j\omega}) + E(e^{j\omega}) \tag{2.23}$$

with

$$\bar{X}(e^{j\omega}) = \breve{H}_0(e^{j\omega}) X(e^{j\omega}) \tag{2.24}$$

is the DTFT of the input signal $X(e^{j\omega})$ multiplied by the average channel frequency responses $\breve{H}_0(e^{j\omega})$ given by

$$\breve{H}_0(e^{j\omega}) = \frac{1}{M} \sum_{m=0}^{M-1} H_m(e^{j\omega}) \tag{2.25}$$

and

$$E(e^{j\omega}) = \sum_{k=1}^{M-1} \breve{Q}_k(e^{j(\omega - k\frac{2\pi}{M})})\bar{X}(e^{j(\omega - k\frac{2\pi}{M})}) \tag{2.26}$$

is the DTFT of the error signal $E(e^{j\omega})$ due to the normalized frequency response mismatch

$$\breve{Q}_k(e^{j\omega}) = \frac{\breve{H}_k(e^{j\omega})}{\breve{H}_0(e^{j\omega})}. \tag{2.27}$$

Now taking the inverse DTFT of (2.23) we get

$$y[n] = \overline{x}[n] + e[n], \tag{2.28}$$

where

$$\overline{x}[n] = \breve{h}_0[n] * x[n], \tag{2.29}$$

and

$$e[n] = \sum_{k=1}^{M-1} \breve{q}_k[n] * \bar{x}[n] e^{jk\frac{2\pi}{M}n}. \tag{2.30}$$

The discrete-time system model of an M-channel TI-ADC represented by (2.38)-(2.30) is shown in Fig. 2.4. The ideally sampled signal $x[n] = x(nT)$ is filtered by the impulse response $\breve{h}_0[n]$ resulting in the desired signal $\overline{x}[n]$. The signal $\overline{x}[n]$ represents the output of an ideal TI-ADC without any frequency response mismatches. Furthermore, we see the error signal $e[n]$, which is the outcome of the signal $\bar{x}[n]$ being first filtered by the discrete-time filters $\breve{q}_k[n]$ and then modulated by $e^{jk\frac{2\pi}{M}n}$, $k = 1, 2, \ldots, M-1$. The filters $\breve{q}_k[n]$ represent the frequency response mismatches in a TI-ADC leading to the error signal $e[n]$. At the output of our system model, the error signal $e[n]$ is added to the desired signal $\bar{x}[n]$ resulting in the distorted TI-ADC output $y[n]$. For the system model discussion we can conclude that we have to remove the error signal $e[n]$ from the TI-ADC output signal $y[n]$ to mitigate the distortions caused by the frequency response mismatches.

Representing the Model as System of Real Filters and Modulators

Even though the signals $\bar{x}[n]$ and $e[n]$ in (2.30) are real signals, the discrete-time filters $\breve{q}_k[n]$ and the modulators $e^{jk\frac{2\pi}{M}n}$ are complex. In order to get a representation

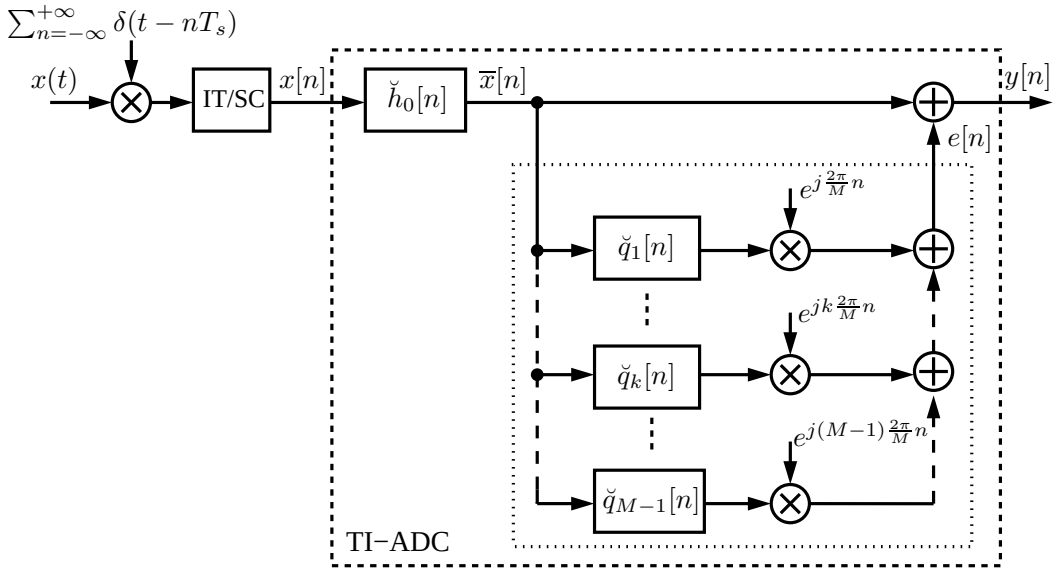

Figure 2.4: *Discrete-time system model of an M-channel TI-ADC. The ideally sampled signal $x[n]$ is filtered by the average channel frequency response $\breve{h}_0[n]$ resulting in the desired signal $\overline{x}[n]$ which is later filtered by the discrete-time filters $\breve{q}_k[n]$, $k = 1, 2, \ldots, M-1$ to produce the error signal $e[n]$ due to the frequency response mismatches. The error $e[n]$ is added to $\overline{x}[n]$ to result in the distorted TI-ADC output $y[n]$.*

for $e[n]$ as a combination of real filters and modulators, we can rewrite (2.30) for an odd number of channels as

$$e[n] = \sum_{k=1}^{(M-1)/2} \left[\breve{q}_k[n] * \bar{x}[n] e^{jk\frac{2\pi}{M}n} + \breve{q}_{M-k}[n] * \bar{x}[n] e^{-jk\frac{2\pi}{M}n} \right]. \tag{2.31}$$

Since

$$\breve{q}_{M-k}[n] = \breve{q}_k^*[n], \tag{2.32}$$

where x^* refers to the complex conjugation of x.

According to [21] the complex impulse response $\breve{q}_k[n]$ can be split into an even and an odd part

$$\breve{q}_k[n] = \breve{q}_k^e[n] + j\breve{q}_k^o[n], \tag{2.33}$$

where $\breve{q}_k^e[n]$ and $\breve{q}_k^o[n]$ are the inverse DTFTs of the frequency responses

$$\breve{Q}_k^e(e^{j\omega}) = \frac{1}{2}(\breve{Q}_k(e^{j\omega}) + \breve{Q}_k^*(e^{-j\omega})) \tag{2.34}$$

and

$$\breve{Q}_k^o(e^{j\omega}) = \frac{1}{2}(\breve{Q}_k(e^{j\omega}) - \breve{Q}_k^*(e^{-j\omega})) \tag{2.35}$$

respectively.

Using (2.32) and (2.33) and the fact that $x + x^* = 2\Re\{x\}$, where $\Re\{x\}$ denotes the real part of x, (2.31) can be rewritten as

$$e[n] = \sum_{k=1}^{(M-1)/2} 2\left[\breve{q}_k^e[n] * \bar{x}[n] \cos\left(k\frac{2\pi}{M}n\right) - \breve{q}_k^o[n] * \bar{x}[n] \sin\left(k\frac{2\pi}{M}n\right) \right]. \tag{2.36}$$

In a similar way we can represent $e[n]$ for an even number of channels M as

$$\begin{aligned} e[n] &= \sum_{k=1}^{M/2-1} 2\left[\breve{q}_k^e[n] * \bar{x}[n] \cos\left(k\frac{2\pi}{M}n\right) - \breve{q}_k^o[n] * \bar{x}[n] \sin\left(k\frac{2\pi}{M}n\right) \right] \\ &+ \breve{q}_{\frac{M}{2}}[n] * \bar{x}[n](-1)^n, \end{aligned} \tag{2.37}$$

where we have an additional real-valued term for $k = \frac{M}{2}$.

Figure 2.5 illustrates $\breve{q}_k[n]$ as a real-valued filter following the representation derived in (2.36) where $e_k[n]$ is the output of the k-th stage of the discrete-time system model of Fig. 2.4. It will be shown in Chapters 3 and 4 that this representation of the filters $\breve{q}_k^e[n]$ and $\breve{q}_k^o[n]$ can be exploited for the adaptive identification and compensation of gain, timing, bandwidth, and frequency response mismatches.

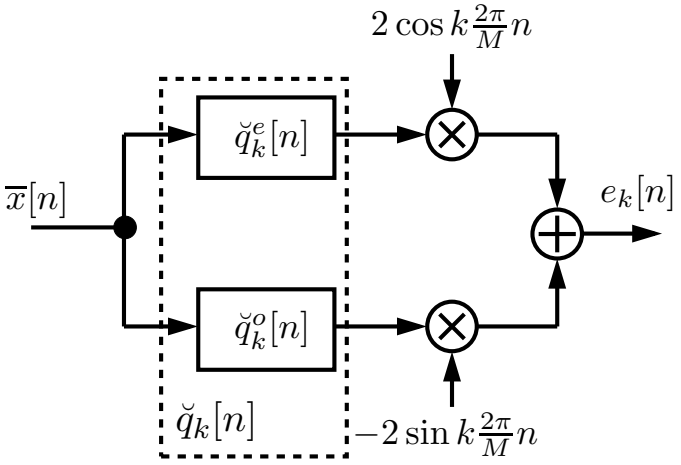

Figure 2.5: *Representation of $\breve{q}_k[n]$ as combination of real-valued filters $\breve{q}_k^e[n]$ and $\breve{q}_k^o[n]$ to get a real-valued error $e_k[n]$ at the output of k-th stage of the discrete-time system model of Fig. 2.4.*

2.4 TI-ADC as an M-Periodic Time-Varying System

As has been shown in Section 2.2 that for each sampling instant $m+lM$ (cf. Fig. 2.3), a different channel with corresponding frequency response $H_m(j\Omega)$, $m = 0, 1, \ldots, M-1$, is active and processes the sample. If all frequency responses $H_m(j\Omega)$ are identical, there is no difference to a single channel ADC. But when there are mismatches among the channels, then for each sampling instant $m + lM$ a different frequency response processes the sample and hence, we have a time-varying system. Moreover, after M sampling instants, the same frequency response is active again. Hence we have an M-periodic time-varying system that accounts for the frequency response mismatches in an M-channel TI-ADC [84]. Next we develop a model to characterize the output $y[n]$ of an M-channel TI-ADC as the output of an M-periodic time-varying system.

After taking the inverse DTFT of (2.20), the output $y[n]$ of an M-channel TI-ADC can be rewritten as

$$y[n] = \sum_{k=0}^{M-1} \sum_{l=-\infty}^{+\infty} \breve{h}_k[l] x[n-l] e^{jkn\frac{2\pi}{M}} \tag{2.38}$$

where

$$\breve{h}_k[l] = \frac{1}{M} \sum_{n=0}^{M-1} h_n[l] e^{-jkn\frac{2\pi}{M}} \tag{2.39}$$

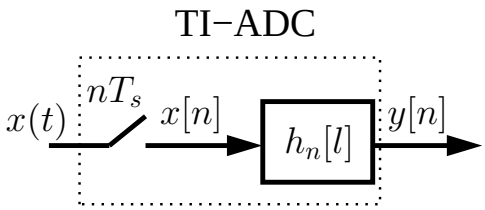

Figure 2.6: *Time-varying system model of a TI-ADC.*

and

$$h_n[l] = \sum_{k=0}^{M-1} \breve{h}_k[l] e^{jkn\frac{2\pi}{M}}. \tag{2.40}$$

From (2.39) and (2.40) it can be noted that $\breve{h}_k[l]$ and $h_n[l]$ form discrete-time Fourier series (DTFS) pairs [21].

Using (2.40) we can simplify (2.38) as

$$y[n] = \sum_{l=0}^{\infty} h_n[l] x[n-l], \tag{2.41}$$

where the starting value of l is 0 since a TI-ADC is a causal system.

From (2.41) it can be concluded that the output $y[n]$ of an M-channel TI-ADC can be generated by passing the input sequence $x[n]$ through a discrete-time time-varying filter with impulse response $h_n[l]$ as shown in Fig. 2.6, where $h_n[l]$ is M-periodic, i.e., $h_n[l] = h_{n+M}[l]$. As will be demonstrated in Chapter 5 that by using an M-periodic time-varying filter in combination with a low-resolution ADC as reference, it is possible to adaptively calibrate frequency response mismatches in an M-channel TI-ADC.

2.5 Conclusions

In this chapter, we have developed the continuous-time, discrete-time, and the time-varying system models of an M-channel TI-ADC. These models characterize the output of a TI-ADC either as the sum of a reference signal without mismatches and an error signal due to the mismatches or as an M-periodic time-varying system. Hence these models analytically represent the effect of mismatches in a TI-ADC and thus can be helpful in designing the calibration techniques to minimize these effects.

3

Adaptive Blind Background Calibration of Gain and Timing Mismatches

In this chapter[1], we present adaptive blind calibration of gain and timing mismatches in a TI-ADC. Gain and timing mismatches in a TI-ADC cause spurious images in its output spectrum thus affecting its performance. We present an efficient digital blind calibration structure to adaptively estimate and correct gain and timing mismatches. Hence the method removes the spurious images from the TI-ADC output spectrum and thus increases the signal-to-noise ratio (SNR). Following methods from the literature [9, 12, 51], we assume a slightly oversampled input signal that helps in the identification of mismatches, but, contrary to them, we can apply our method to an arbitrary number of channels in a straightforward way as will be explained later.

After a brief introduction in Section 3.1, we approximate the discrete-time system model of a TI-ADC presented in Chapter 2 with a truncated Taylor's series in Section 3.2 that helps in getting a representation for the output of a TI-ADC suffering from gain and timing mismatches. In Section 3.3 we first introduce the main idea of the blind calibration and later we present the design of the blind calibration structure that estimates and compensates the gain and timing mismatches. Section 3.4 demonstrates the performance of the blind calibration structure through numerical examples while we conclude the chapter in Section 3.5.

3.1 Introduction

Gain and timing mismatches are special cases of frequency response mismatches. Gain mismatches are a form of magnitude response mismatches except that their value does not depend on input signal frequency. They arise when each channel ADC has a different

[1]Parts of this chapter have been published in [14, 17]

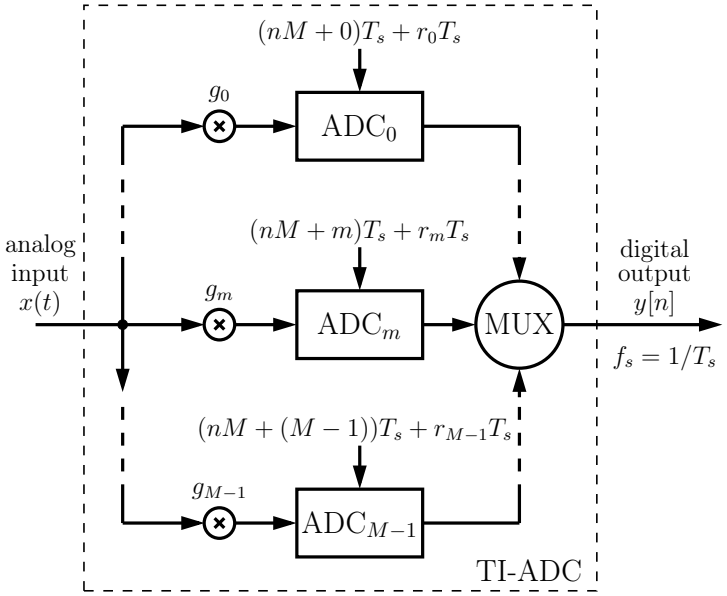

Figure 3.1: *Model of an M-channel TI-ADC with gains g_m and the relative timing offsets r_mT_s for $m = 0, 1, \ldots, M-1$.*

gain. The timing mismatches are linear phase mismatches that cause a deterministic deviation between the ideal sampling period and the real sampling period if several channel ADCs are combined. An M-channel TI-ADC with each channel ADC being characterized by the gain g_m and the relative timing offset r_mT_s for $m = 0, 1, \ldots, M-1$ is shown in Fig. 3.1. For an ideal TI-ADC without gain and timing mismatches $g_m = 1$ and $r_m = 0$. The effect of gain and timing mismatches on the sampling process of a four-channel TI-ADC is depicted in Fig. 3.2.

In recent years, calibration of gain and timing mismatches in a TI-ADC have been considered in [10–12, 43]. There are few other methods where only the calibration of timing mismatches have been presented [8, 9, 13, 51, 54, 85].

The calibration methods presented in [11, 12, 43] deal with a two-channel TI-ADC only. In [43], the authors have presented a digital background calibration structure for the offset, gain, and timing mismatches. They reported a sampling rate of 120 MS/s with 10-bit resolution. The power dissipation was 234 mW. In [11] gain and timing mismatches have been estimated by minimizing the norm of the autocorrelation function of a TI-ADC output. Later the estimated values have been used to design correction filters that can reconstruct the input signal. In [12] authors have used a multirate filter bank structure to model mismatches. By using the digital fractional

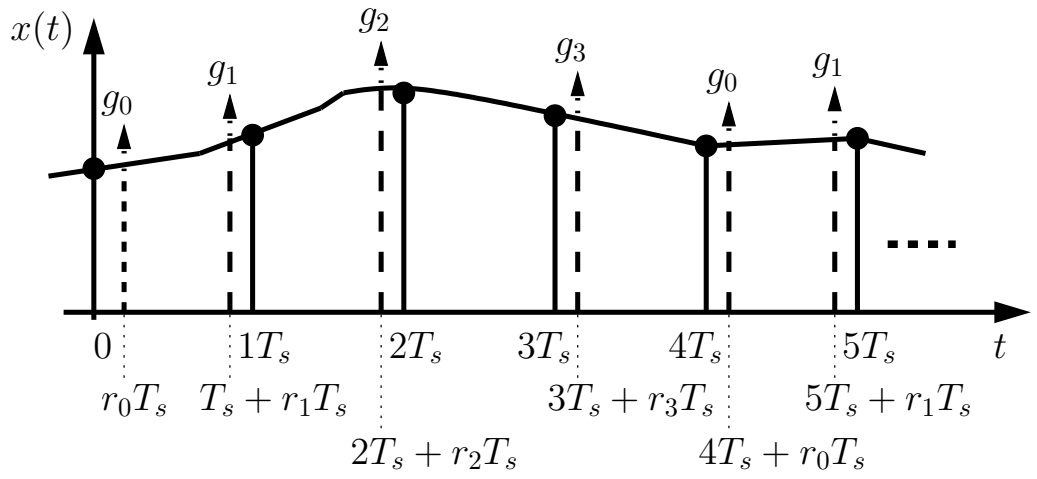

Figure 3.2: *Effect of gain and timing mismatches on the sampling process of a four-channel TI-ADC ($M = 4$).*

delay filters in combination with an ideal low-pass filter timing and gain mismatches have been estimated. Later the reconstructed input signal has been obtained by using the correction filters. In [10], the authors have investigated blind adaptive equalization of offset, gain, and timing mismatches in an M-channel TI-ADC. First they developed the corresponding loss functions for each of the individual mismatches, and later they have got the respective mismatch estimates by minimizing those loss functions. Nevertheless, the performance of this technique has been demonstrated for a multitone input signal only. Furthermore, they have used a gradient minimization algorithm to adaptively estimate the mismatches that itself requires a lot of computations.

The blind calibration method presented in this chapter requires a bandlimited and oversampled input signal just like the other methods reviewed above. Contrary to them, however, we use a structure that does not require any correction filters. For the identification of gain and timing mismatches, we use the FxLMS algorithm [81, 82]. The estimated gain and timing mismatches are utilized to produce an estimated error signal. The estimated error signal is subtracted from the TI-ADC output to give us the reconstructed input signal as shown in [53].

In order to get explicit representations for the reference and the error signals in the presence of gain and timing mismatches, we will first approximate the discrete-time system model of Chapter 2 by applying a first-order Taylor's series approximation to the channel frequency responses. This approximated system model will be later utilized to design the blind calibration structure for gain and timing mismatches.

3.2 Taylor's Series Approximated System Model

Using the discrete-time system model of a TI-ADC developed in Chapter 2, we can represent the discrete-time channel frequency response $H_m(e^{j\omega})$ for the case of gain and timing mismatches as

$$H_m(e^{j\omega}) = g_m e^{H_d(e^{j\omega})r_m}, \tag{3.1}$$

where

$$H_d(e^{j\omega}) = j\omega \text{ for } -\pi < \omega \leq \pi \tag{3.2}$$

is the frequency response of the ideal discrete-time differentiator [21].

Hence using (3.1) and (2.20)-(2.21), we can rewrite the discrete-time output $Y(e^{j\omega})$ of a TI-ADC suffering from gain and timing mismatches as

$$Y\left(e^{j\omega}\right) = \sum_{k=0}^{M-1} \breve{H}_k\left(e^{j\left(\omega - k\frac{2\pi}{M}\right)}\right) X\left(e^{j\left(\omega - k\frac{2\pi}{M}\right)}\right) \tag{3.3}$$

with

$$\breve{H}_k\left(e^{j\omega}\right) = \frac{1}{M}\sum_{m=0}^{M-1} g_m e^{H_d\left(e^{j\omega}\right)r_m} e^{-jk\frac{2\pi}{M}m}. \tag{3.4}$$

Since in a typical TI-ADC the relative time offsets r_m are small compared to the sampling period T_s, a first-order Taylor's series approximation can be applied to the term $e^{r_m Hd(e^{j\omega})}$ by neglecting the higher order terms, which results in

$$e^{H_d\left(e^{j\omega}\right)r_m} \approx 1 + H_d\left(e^{j\omega}\right) r_m. \tag{3.5}$$

After substituting (3.5) in (3.4) we get

$$\breve{H}_k\left(e^{j\omega}\right) = G_k + R_k H_d\left(e^{j\omega}\right) \tag{3.6}$$

with

$$\begin{aligned} G_k &= \frac{1}{M}\sum_{m=0}^{M-1} g_m e^{-jk\frac{2\pi}{M}m}, \\ R_k &= \frac{1}{M}\sum_{m=0}^{M-1} g_m r_m e^{-jk\frac{2\pi}{M}m}. \end{aligned} \tag{3.7}$$

Substituting (3.6) in (3.3) gives

$$Y(e^{j\omega}) = \bar{X}(e^{j\omega}) + E(e^{j\omega}) \tag{3.8}$$

with

$$\bar{X}(e^{j\omega}) = (G_0 + R_0 H_d\left(e^{j\omega}\right))X(e^{j\omega}) \tag{3.9}$$

where $(G_0 + R_0 H_d\left(e^{j\omega}\right))$ is the average response among all channels and

$$E(e^{j\omega}) = \sum_{k=1}^{M-1} \left[G_k X\left(e^{j\left(\omega - k\frac{2\pi}{M}\right)}\right) + R_k H_d\left(e^{j\left(\omega - k\frac{2\pi}{M}\right)}\right) X\left(e^{j\left(\omega - k\frac{2\pi}{M}\right)}\right)\right]. \tag{3.10}$$

is the error introduced by gain and timing mismatches.

Without loss of generality, it can be assumed that the average value of all timing mismatches r_m is zero, since an overall delay does not introduce any mismatch effects. Accordingly, and with the further assumption that the gain mismatches are small, i.e, $g_0 \sim g_1 \sim, \sim \ldots \sim g_{M-1}$, then R_0 in (3.9) is close to zero as well and can be neglected. The inverse discrete-time Fourier transform of (3.8) can therefore be written as

$$y[n] = \bar{x}[n] + e[n] \tag{3.11}$$

with

$$\bar{x}[n] = G_0 x[n] \tag{3.12}$$

and

$$e[n] = \sum_{k=1}^{M-1} \left[G_k \cdot x[n] e^{jk\frac{2\pi}{M}n} + R_k \cdot h_d[n] * x[n] e^{jk\frac{2\pi}{M}n}\right]. \tag{3.13}$$

Since the modulators $e^{jk\frac{2\pi}{M}n}$ are complex, hence following the analysis in Section 2.3 of Chapter 2, the error $e[n]$ can be expressed for even M as

$$e[n] = \sum_{k=1}^{\frac{M}{2}-1} e_k[n] + e_{\frac{M}{2}}[n]. \tag{3.14}$$

where

$$\begin{aligned} e_k[n] &= 2\left[\Re\{G_k\}\cos\left(k\frac{2\pi}{M}n\right) - \Im\{G_k\}\sin\left(k\frac{2\pi}{M}n\right)\right] x[n] \\ &+ 2\left[\Re\{R_k\}2\cos\left(k\frac{2\pi}{M}n\right) - \Im\{R_k\}\sin\left(k\frac{2\pi}{M}n\right)\right] h_d[n] * x[n] \end{aligned} \tag{3.15}$$

and

$$e_{\frac{M}{2}}[n] = G_{\frac{M}{2}}(-1)^n x[n] + R_{\frac{M}{2}}(-1)^n h_d[n] * x[n], \tag{3.16}$$

where $\Re\{x\}$ is the real part of x and $\Im\{x\}$ is the imaginary part of x. For the case of a two-channel TI-ADC, i.e., $M = 2$, the error $e[n]$ equals (3.16).

By introducing the coefficient vectors

$$\mathbf{c}_g = \left(\Re\{G_1\}, \Im\{G_1\}, \ldots, \Re\{G_k\}, \Im\{G_k\}, \ldots, \Re\{G_{\frac{M}{2}-1}\}, \Im\{G_{\frac{M}{2}-1}\}, G_{\frac{M}{2}}\right)^T \quad (3.17)$$

$$\mathbf{c}_r = \left(\Re\{R_1\}, \Im\{R_1\}, \ldots, \Re\{R_k\}, \Im\{R_k\}, \ldots, \Re\{R_{\frac{M}{2}-1}\}, \Im\{R_{\frac{M}{2}-1}\}, R_{\frac{M}{2}}\right)^T \quad (3.18)$$

and the modulation vector

$$\begin{aligned}\mathbf{m}[n] = \Bigg[&2\cos\left(1\frac{2\pi}{M}n\right), -2\sin\left(1\frac{2\pi}{M}n\right), \ldots, \\ &2\cos\left(k\frac{2\pi}{M}n\right), -2\sin\left(k\frac{2\pi}{M}n\right), \ldots, \\ &2\cos\left(\left(\frac{M}{2}-1\right)\frac{2\pi}{M}n\right), -2\sin\left(\left(\frac{M}{2}-1\right)\frac{2\pi}{M}n\right), (-1)^n\Bigg)^T\end{aligned} \quad (3.19)$$

the signal vectors can be defined as

$$\mathbf{x}_g[n] = \mathbf{m}[n]x[n] \quad (3.20)$$

and

$$\mathbf{x}_r[n] = \mathbf{m}[n]h_d[n] * x[n]. \quad (3.21)$$

Therefore, the error $e[n]$ in (3.14) can finally be written in vector notation as

$$e[n] = \mathbf{c}_g^T\mathbf{x}_g[n] + \mathbf{c}_r^T\mathbf{x}_r[n]. \quad (3.22)$$

The first-order Taylor's series approximated discrete-time system model of an M-channel TI-ADC represented by (3.11) is shown in Fig. 3.3.

3.3 Adaptive Blind Calibration

In this section we present the design of the blind calibration structure as shown in Fig. 3.4 to estimate gain and timing mismatches. In general, this structure requires a differentiator, $2(M-1)$ modulators, $2(M-1)$ time-varying multipliers, and a single high-pass filter. It gives the estimated gain and timing offset coefficient vectors $\hat{\mathbf{c}}_g$ and $\hat{\mathbf{c}}_r$ by using the FxLMS algorithm. The need for the FxLMS algorithm arises because of the high-pass filter $f[n]$ in the error-path of the blind calibration structure as shown in Fig. 3.4. Therefore, the FxLMS algorithm uses the filtered reference and error signals that help in increasing the convergence rate of the standard LMS algorithm [81, 82]. The estimated values generated by the FxLMS algorithm help in getting an estimated

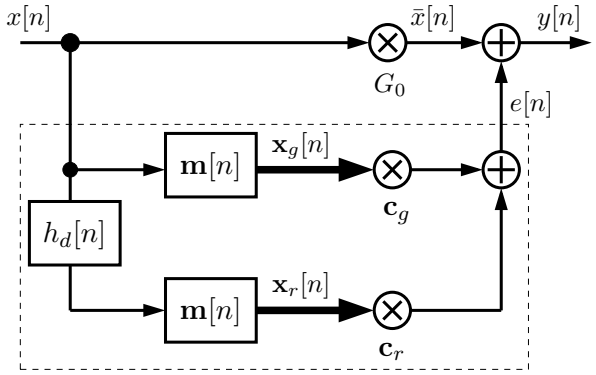

Figure 3.3: *The first-order Taylor's series approximated discrete-time system model of an M-channel TI-ADC with gain and timing mismatches.*

error signal $\hat{e}[n]$ that is subtracted from $y[n]$ to get the reconstructed input signal $\hat{x}[n]$ as

$$\begin{aligned} \hat{x}[n] &= y[n] - \hat{e}[n] \\ &= G_0 x[n] + e[n] - \hat{e}[n]. \end{aligned} \tag{3.23}$$

where

$$\hat{e}[n] = \hat{\mathbf{c}}_g^T[n]\mathbf{y}_g[n] + \hat{\mathbf{c}}_r^T[n]\mathbf{y}_r[n]. \tag{3.24}$$

with

$$\begin{aligned} \mathbf{y}_g[n] &= \mathbf{m}[n]y[n] \\ \mathbf{y}_r[n] &= \mathbf{m}[n]y[n] * h_d[n]. \end{aligned} \tag{3.25}$$

3.3.1 Main Idea

For blind identification, the bandlimited input signal with bandwidth B is slightly over-sampled leading to the creation of a frequency band in the TI-ADC output spectrum near half the sampling frequency $\Omega_s/2$, known as the mismatch band. This mismatch band only contains the aliasing components due to $e[n]$ as shown in Fig. 3.5 for a four channel TI-ADC.

By minimizing the error signal energy in the mismatch band it is possible to adaptively identify the coefficient vectors $\hat{\mathbf{c}}_g$ and $\hat{\mathbf{c}}_r$ by using the FxLMS algorithm as

$$\begin{aligned} \hat{\mathbf{c}}_g[n] &= \hat{\mathbf{c}}_g[n-1] + \mu_g \mathbf{y}_g[n-D]\varepsilon[n] \\ \hat{\mathbf{c}}_r[n] &= \hat{\mathbf{c}}_r[n-1] + \mu_r \mathbf{y}_r[n-D]\varepsilon[n], \end{aligned} \tag{3.26}$$

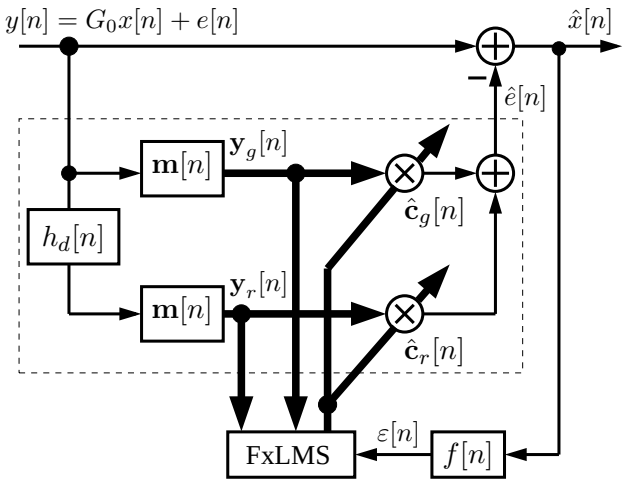

Figure 3.4: *The proposed adaptive blind calibration structure for gain and timing mismatches.*

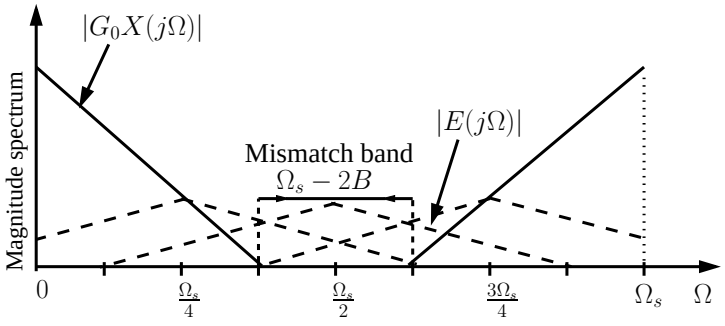

Figure 3.5: *Main idea of blind identification for a four-channel TI-ADC, where $G_0X(j\Omega)$ (solid lines) and $E(j\Omega)$ (dashed lines) are continuous-time Fourier transforms (CTFT) of $G_0x[n]$ and $e[n]$ respectively.*

where $\varepsilon[n]$ is the error signal of the blind identification structure (cf. Fig. 3.4), $\mathbf{y}_g[n-D]$ and $\mathbf{y}_r[n-D]$ are delayed versions of $\mathbf{y}_g[n]$ and $\mathbf{y}_r[n]$ with D denoting the delay of the high-pass filter $f[n]$, whereas μ_g and μ_r are the step-size parameters for the FxLMS algorithm. It should be noted that the FxLMS algorithm actually requires high-pass filtered version of $\mathbf{y}_g[n]$ and $\mathbf{y}_r[n]$, but in order to reduce the implementation complexity it is demonstrated in Section 3.4 that simply delaying the signals is sufficient.

3.3.2 Analysis

To estimate gain and timing mismatches, we use a single high-pass filter $f[n]$ that attenuates the input signal energy in $\hat{x}[n]$ to leave only the mismatch band, i.e.

$$\varepsilon[n] \;=\; \hat{x}[n] * f[n]. \tag{3.27}$$

Substituting (3.23) in (3.27) gives

$$\varepsilon[n] \;=\; G_0 x[n] * f[n] + e[n] * f[n] - \hat{e}[n] * f[n]. \tag{3.28}$$

Since $f[n]$ strongly attenuates $G_0 x[n]$, we are left with

$$\begin{aligned} \varepsilon[n] &\approx e[n] * f[n] - \hat{e}[n] * f[n] \\ &\approx e_f[n] - \hat{e}_f[n], \end{aligned} \tag{3.29}$$

where

$$e_f[n] \;=\; e[n] * f[n] \tag{3.30}$$

and

$$\hat{e}_f[n] \;=\; \hat{e}[n] * f[n]. \tag{3.31}$$

Substituting (3.22) in (3.30) gives

$$e_f[n] \;=\; \mathbf{c}_g^T \overline{\mathbf{x}}_g[n] + \mathbf{c}_r^T \overline{\mathbf{x}}_r[n], \tag{3.32}$$

where

$$\overline{\mathbf{x}}_g[n] \;=\; \mathbf{m}[n] x[n] * f[n] \tag{3.33}$$

$$\overline{\mathbf{x}}_r[n] \;=\; \mathbf{m}[n] x[n] * h_d[n] * f[n]. \tag{3.34}$$

In a typical TI-ADC where the input signal energy is significantly greater than the mismatch signal energy, therefore, for a first order analysis, we can approximate $\mathbf{y}_g[n]$ and $\mathbf{y}_r[n]$ in (3.25) by using (3.20)-(3.21) as

$$\begin{aligned} \mathbf{y}_g[n] &\approx G_0 \mathbf{x}_g[n] \\ \mathbf{y}_r[n] &\approx G_0 \mathbf{x}_r[n] \end{aligned} \tag{3.35}$$

and consequently $\hat{e}[n]$ in (3.24) as

$$\hat{e}[n] \approx G_0\hat{\mathbf{c}}_g^T[n]\mathbf{x}_g[n] + G_0\hat{\mathbf{c}}_r^T[n]\mathbf{x}_r[n]. \tag{3.36}$$

Substituting (3.36) in (3.31) gives

$$\hat{e}_f[n] = G_0\hat{\mathbf{c}}_g^T[n]\overline{\mathbf{x}}_g[n] + G_0\hat{\mathbf{c}}_r^T[n]\overline{\mathbf{x}}_r[n]. \tag{3.37}$$

Substituting (3.32) and (3.37) in (3.29) and simplifying gives

$$\varepsilon[n] = G_0\left(\frac{1}{G_0}\mathbf{c}_g - \hat{\mathbf{c}}_g[n]\right)^T\overline{\mathbf{x}}_g[n] + G_0\left(\frac{1}{G_0}\mathbf{c}_r - \hat{\mathbf{c}}_r[n]\right)^T\overline{\mathbf{x}}_r[n]. \tag{3.38}$$

If the estimated coefficients vectors $\hat{\mathbf{c}}_g[n]$ and $\hat{\mathbf{c}}_r[n]$ match $\mathbf{c}_g$ and $\mathbf{c}_r$, i.e.,

$$\begin{aligned}\hat{\mathbf{c}}_g[n] &= \frac{1}{G_0}\mathbf{c}_g \\ \hat{\mathbf{c}}_r[n] &= \frac{1}{G_0}\mathbf{c}_r\end{aligned} \tag{3.39}$$

then $\varepsilon[n] \approx 0$.

Finally the reconstructed input signal $\hat{x}[n]$ can be obtained by substituting (3.22) and (3.36) and simplifying

$$\hat{x}[n] \approx G_0x[n] + G_0\left(\frac{1}{G_0}\mathbf{c}_g - \hat{\mathbf{c}}_g[n]\right)^T\overline{\mathbf{x}}_g[n] + G_0\left(\frac{1}{G_0}\mathbf{c}_r - \hat{\mathbf{c}}_r[n]\right)^T\overline{\mathbf{x}}_r[n]. \tag{3.40}$$

If (3.39) holds then

$$\hat{x}[n] \approx G_0x[n] \tag{3.41}$$

and the reconstructed input signal does not contain any signals due to the mismatches.

3.4 Simulation Results

To illustrate the performance of the proposed adaptive calibration structure we have simulated a 4-channel TI-ADC with gain and timing mismatches as shown in 3.1. For the given gain and timing mismatches given in Tab.3.1, the corresponding values of $\mathbf{c}_g$ and $\mathbf{c}_r$ were computed by using (3.17) and (3.18) as

$$\mathbf{c}_g = [0.005, 0.001, 0] \tag{3.42}$$

and

$$\mathbf{c}_r = [-0.001, 0.0015, 0.00014]. \tag{3.43}$$

Table 3.1: *Simulated gain and timing mismatch values*

ADC	g_m	r_m
ADC_0	1.01	$-0.007T_s$
ADC_1	0.98	$+0.002T_s$
ADC_2	0.99	$-0.003T_s$
ADC_3	1.02	$+0.008T_s$

The differentiator $h_d[n]$ was designed using the Matlab function 'firpm' whereas the high-pass filter $f[n]$ was an equiripple filter designed by using the Matlab filter design tool 'fdatool'. The number of taps for both $h_d[n]$ and $f[n]$ were 33. The overall performance of the blind structure was characterized by the signal-to-noise ratio (SNR) for $y[n]$ as

$$\text{SNR} = 10\log_{10}\left(\frac{\sum_{n=0}^{N-1}|G_0x[n]|^2}{\sum_{n=0}^{N-1}|G_0x[n]-y[n]|^2}\right) \tag{3.44}$$

and for $\hat{x}[n]$ as

$$\text{SNR} = 10\log_{10}\left(\frac{\sum_{n=0}^{N_1-1}|G_0x[n]|^2}{\sum_{n=0}^{N_1-1}|G_0x[n]-\hat{x}[n]|^2}\right), \tag{3.45}$$

where N denotes the number of samples used to calculate the SNR before calibration, and N_1 denotes the number of samples used to calculate the SNR after calibration (once the FxLMS algorithm has converged).

3.4.1 Bandlimited White Gaussian Noise Input Signal

First we simulated a bandlimited white Gaussian noise (WGN) input signal with bandwidth $0.7\frac{\Omega_s}{2}$ and variance $\sigma = 1$. We took $N = 2^{20}$ samples of the input signal. The step size parameters μ_r and μ_g for FxLMS were chosen as 0.01. This choice of μ_r and μ_g is based on the experimentation, however, their values lie within the stability bounds of FxLMS algorithm, as specified in [81, 82]. Same is true about the value of μ_r and μ_g in the next simulation example that considers a bandlimited multitone input signal. The corresponding cutoff frequencies of $f[n]$ and $h_d[n]$ were set to 0.7π.

Figure 3.6 shows the energy density spectrum of $y[n]$ (last $N_1 = 2^{11}$ samples out of the 2^{20} samples), where the SNR was about 35.2 dB. In Fig. 3.7 the energy density spectrum of $\hat{x}[n]$ (last $N_1 = 2^{11}$ samples) is shown once the FxLMS algorithm has converged. The computed value of the SNR was 69.3 dB, hence, leading to an improvement of almost 34.1 dB.

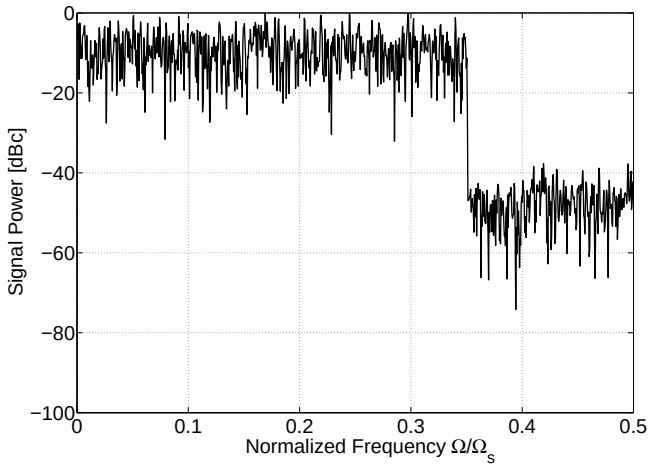

Figure 3.6: *Power spectrum of the uncalibrated output $y[n]$ for the case of a WGN input signal bandlimited to $0.7\frac{\Omega_s}{2}$. The SNR was computed as 35.2 dB.*

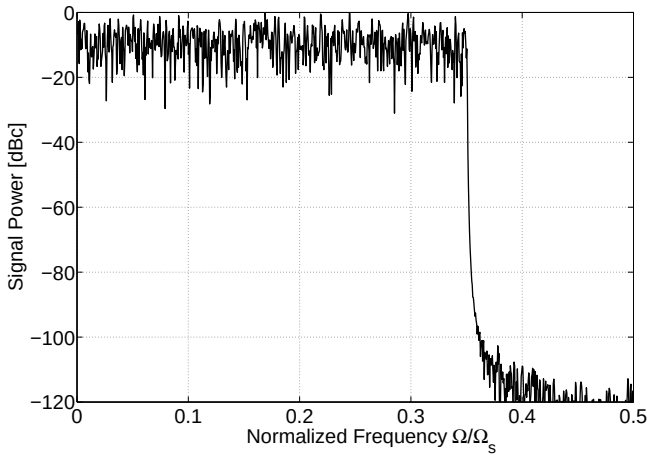

Figure 3.7: *Power spectrum of the reconstructed input signal $\hat{x}[n]$. The value of the SNR once the FxLMS algorithm converged was 69.3 dB which is an improvement of 34.1 dB.*

The convergence behavior of the estimated gain coefficients vector $\hat{\mathbf{c}}_g[n]$ and the timing offset coefficients vector $\hat{\mathbf{c}}_r[n]$ are shown in Fig. 3.8 and Fig. 3.9 respectively. As can be seen $\hat{\mathbf{c}}_g[n]$ and $\hat{\mathbf{c}}_r[n]$ correspond well to $\mathbf{c}_g$ and $\mathbf{c}_r$.

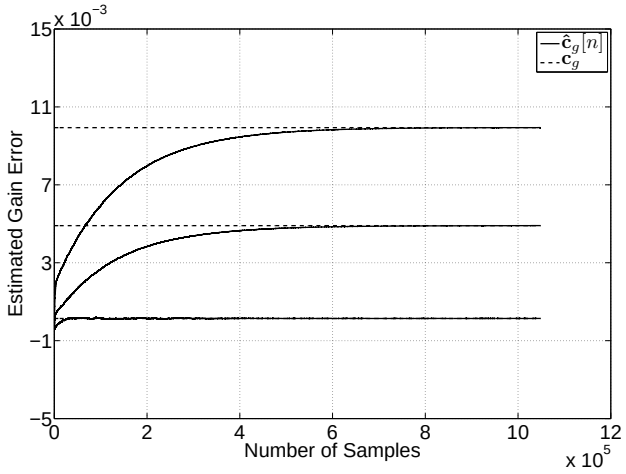

Figure 3.8: *The convergence behavior of the estimated gain mismatch coefficients $\hat{\mathbf{c}}_g[n]$ (solid lines) for the case of bandlimited WGN input signal, compared to their expected values (dashed lines) as given by (3.42).*

3.4.2 Bandlimited Multitone Input Signal

Next we simulated a multitone input signal with 42 sinusoids bandlimited to $0.8\frac{\Omega_s}{2}$ and having constant amplitudes, uniformly spaced frequencies, and random phases. Once again we took $N = 2^{20}$ samples of the input signal. The cutoff frequencies of $f[n]$ and $h_d[n]$ were set to 0.8π. The step sizes μ_g and μ_r were both chosen as 0.0001.

The power spectra of the uncompensated output $y[n]$ and the reconstructed input signal $\hat{x}[n]$ are shown in Fig. 3.10 and 3.11, respectively. It can be seen that not only the energy in the mismatch band is reduced considerably but also the energy of the aliasing components that are overlapping with the input signal spectra has been minimized. the computed SNR value for $y[n]$ was 35 dB while for $\hat{x}[n]$ it was 67.3 dB, which in fact was an improvement of almost 32.3 dB.

The convergence behavior of the estimated gain and timing mismatch coefficient vectors, i.e., $\hat{\mathbf{c}}_g[n]$ and $\hat{\mathbf{c}}_r[n]$ are shown in Fig. 3.12 and 3.13, respectively. Both $\hat{\mathbf{c}}_g[n]$ and $\hat{\mathbf{c}}_r[n]$ have nicely converged to their computed values given by (3.42) and (3.43), respectively.

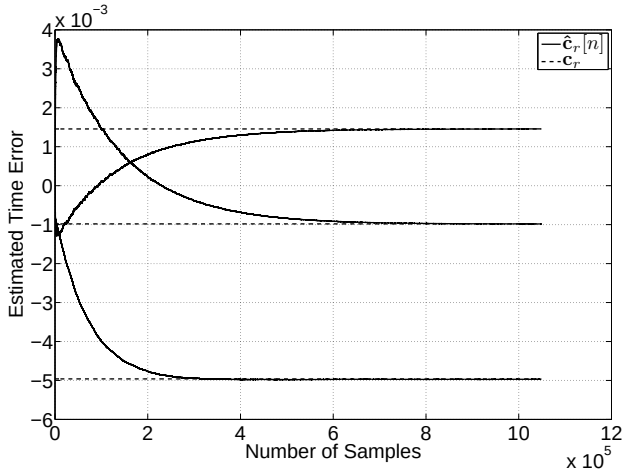

Figure 3.9: *The convergence behavior of the estimated timing mismatch coefficients* $\hat{\mathbf{c}}_r[n]$ *(solid lines) for the case of bandlimited WGN input signal, compared to their expected values (dashed lines) as given by (3.43).*

3.5 Conclusions

In this chapter we have presented an efficient blind identification structure for gain and timing mismatches in an M-channel TI-ADC. The identification is based on the FxLMS algorithm that uses a single high-pass filter. While using the bandlimited WGN and multitone input signals, we have identified gain and timing mismatches in a 4-channel TI-ADC that has led to a significant improvement in the SNR. The proposed blind identification structure can be scaled to an arbitrary number of channel ADCs, where the complexity linearly scales with the number of channels. For each additional channel ADC, we only need two modulators and two multipliers for scaling. Hence we have an efficient calibration structure that requires minimum extra hardware if additional channel ADCs are added.

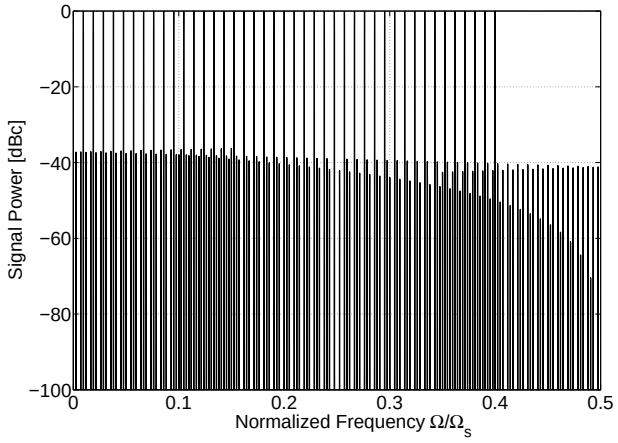

Figure 3.10: *Power spectrum of the uncalibrated output* $y[n]$ *for the case of a multitone input signal with* 42 *sinusoids bandlimited to* $0.8\frac{\Omega_s}{2}$ *and having constant amplitudes, uniformly spaced frequencies, and random phases. The SNR is* 35 *dB.*

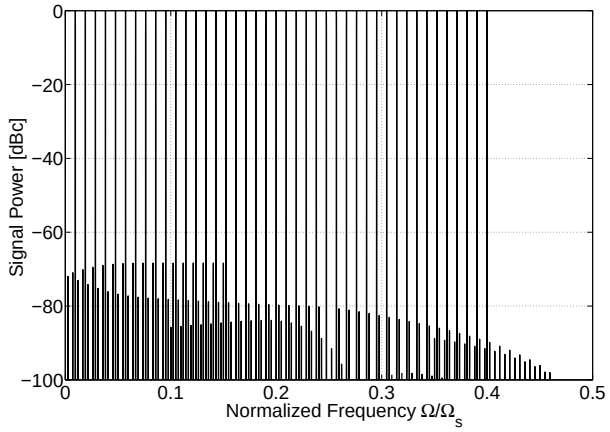

Figure 3.11: *Power spectrum of the reconstructed output* $\hat{x}[n]$ *using a* $1st$ *order calibration structure. The SNR is* 69.2 *dB which is an improvement of* 34.2 *dB.*

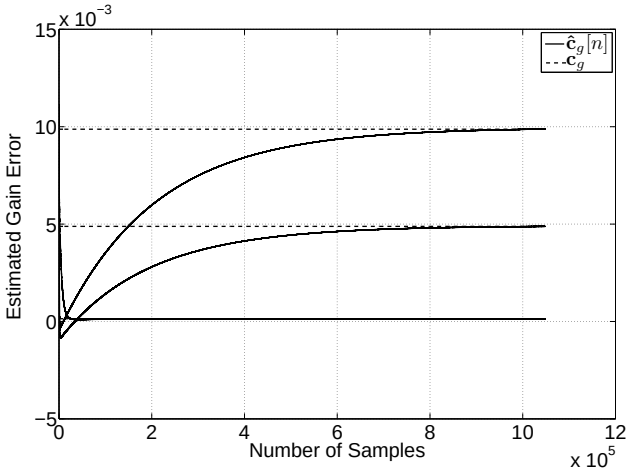

Figure 3.12: *The convergence behavior of the estimated gain mismatch coefficients* $\hat{\mathbf{c}}_g[n]$ *(solid lines) for the case of a multitone input signal, compared to their expected values (dashed lines) as given by (3.42).*

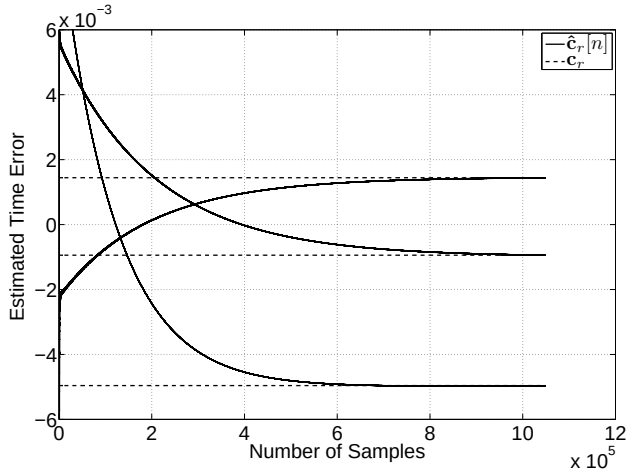

Figure 3.13: *The convergence behavior of the estimated timing mismatch coefficients* $\hat{\mathbf{c}}_r[n]$ *(solid lines) for the case of a multitone input signal, compared to their expected values (dashed lines) as given by (3.43).*

4

Adaptive Blind Background Calibration of Frequency Response Mismatches Represented by Polynomials

This chapter[1] introduces an adaptive calibration structure for the blind calibration of frequency response mismatches in a two-channel TI-ADC. By representing frequency response mismatches as polynomials, we can exploit slight oversampling, to estimate the coefficients of the polynomials by using the FxLMS algorithm. Utilizing the coefficients in the adaptive structure, we can compensate frequency response mismatches including time offset and bandwidth mismatches. We develop an analytical framework for the calibration structure and analyze its performance.

At this stage we would also like to highlight the main differences between the blind calibration methods presented in this chapter and in chapter 3. In chapter 3 we have used a first order Taylor's series approximation for the channel frequency response mismatches while in this chapter we use a polynomial series of fixed order to model the mismatches. Moreover, the method in chapter 3 was only applicable to special form of channel frequency response mismatches, i.e., gain and timing mismatches while in current chapter we present a method that can handel different types of channel frequency response mismatches including gain, and timing mismatches.

After the introduction in 4.1, Section 4.2 develops a polynomial representation of the normalized frequency response mismatches using a p-th order polynomial. Based on this polynomial approximation we present the design of the calibration structure in Section 4.3, which includes the calibration principle, the calibration structure, the identification algorithm, and a performance analysis. In Sec. 4.4 simulation results

[1] Parts of this chapter have been published in [15]

show the performance of the calibration method by using different examples from the literature.

4.1 Introduction

In this chapter we study the digital correction of frequency response mismatches, since digital postcorrection techniques of analog circuits are getting increasingly attractive [3] and can pave the way to high-resolution TI-ADCs [5].

In recent years, the digital calibration of frequency response mismatches has been considered in [64–67, 69, 70, 72], as this can lead to further improvement in the overall performance of TI-ADCs [5]. In [67] a method to compensate frequency response mismatches based on multi-rate theory and least-squares filter design is presented. The approach works well, but the required special calibration signals and the high complexity of the filter design limit this approach to applications where time-consuming extra calibration cycles are tolerable [86]. A different least-squares filter design method for frequency response mismatches is presented in [72]. The correction of bandwidth mismatches for a two-channel TI-ADC was first introduced in [66], where the correction is basically done as in [67]. A more comprehensive model to correct bandwidth mismatches in a two-channel TI-ADC was developed in [64]. In contrast to [66] the authors also introduce a tailored correction based on a single FIR filter that further reduces the design complexity. By injecting a test tone of some known frequency below the Nyquist frequency the same authors have shown in [65] an adaptive way to estimate the bandwidth mismatches in a two-channel TI-ADC. The compensation of magnitude response mismatches in TI-ADCs was presented in [69, 70] and further developed to the compensation of frequency response mismatches in [71]. Compared to other methods as for example to [67], the methods have a reduced filter design complexity. In particular, for frequency response mismatches where the mismatches only depend on a single free parameter like the time offsets or the bandwidth, the method leads to very efficient filter structures [52, 53, 71] that can be adapted in real-time [16, 80]. However, it was not shown in [71] how to extend this structure to the calibration of more general frequency response mismatches. The compensation of frequency response mismatches by using polynomial representations has been investigated in [63, 74, 75]. In [63, 74] the authors have presented a blind calibration structure based on a multirate filter bank for a two-channel TI-ADC. The authors need to know channel frequency responses analytically to derive the analysis filters, which are weighted by coefficients to be identified.

Unfortunately, this work has not further been presented in a more comprehensive manner, which would allow to decide on the quality and the validity of the identification procedure. In [75] a compensation structure based on polynomial approximations for frequency response mismatches is introduced. The proposed structure uses differentiators and variable multipliers corresponding to the parameters in polynomial models of the channel frequency responses. Unfortunately, the paper does not discuss the identification of these parameters.

The main features of our calibration approach are as follows.

Polynomial model of frequency response mismatches

We use a P-th order polynomial to model the frequency response mismatches in a two-channel TI-ADC. This is an approach similar to the one presented in [75], where the authors have modeled the frequency responses as polynomial series. The basic assumption of our model approach is that for a certain TI-ADC design we can identify a model order P, which does not change over different chip realizations and time. Accordingly, the change of frequency response mismatches, for example, over time can be described by a change of the coefficients of a polynomial series of order P.

Adaptive calibration structure

We present a calibration structure that exploits the adaptability of the polynomial representation of frequency response mismatches. It, therefore, extends the structure presented in [71], which can reconstruct the ideally sampled signal, but was not adaptable to general frequency response mismatches.

Blind adaptive background calibration

By combining the calibration structure with the spectral properties of slightly oversampled input signals, we can show how to utilize the filtered error least-mean square (FxLMS) algorithm [81, 82] to blindly identify frequency response mismatches and, consequently, exploit the identified frequency response mismatches to remove the mismatch artifacts from the TI-ADC output signal.

Remarks on the Calibration Method

The proposed calibration method requires that the spectrum of the sampled signal contains a region which we call the mismatch band and where no significant signal energy is present. The simplest option is to oversample the bandlimited analog input signal,

where we obtain a mismatch band close to the Nyquist frequency. This option is also utilized in this chapter. The mismatch band, however, can be at any other position in the frequency band or can even consist of non connected regions[59]. To this end, the used filter for the mismatch band in the calibration method has to be adapted appropriately. Moreover, as long as there is a mismatch band, the method can also work if the input signal lies even in the other Nyquist zones.

Another requirement is that the input signal contributes significant error energy to the mismatch band. Narrow band signals or even sinusoidal input signals do not fullfill this criterion, but for such signals we can either use a simple filter to remove the mismatches or, if we are interested in the mismatches, can use simple and very precise identification methods [32, 59].

We represent the frequency response mismatches using a polynomial series. On the one hand, the coefficients of the polynomial do not directly correspond to typical mismatch parameters such as the bandwidth, which could be a drawback. On the other hand, we obtain a model that is linear in its parameters and we can use simple algorithms like the FxLMS to identify the coefficients.

The calibration method identifies and corrects the mismatches in the digital domain. Although a multi-rate implementation is possible, an analog tuning of the parameters [50, 86] is likely to be more energy efficient, but does not have the flexibility and accuracy of digital methods [3].

4.2 Polynomial Representation of Frequency Response Mismatches

Starting with the discrete-time system model of an M-channel TI-ADC developed in Chapter 2, the error $e[n]$ given by (2.30) is simplified for a two-channel TI-ADC as

$$e[n] \quad = \quad \breve{q}[n] * \bar{x}[n](-1)^n. \tag{4.1}$$

This simplification leads to discrete-time system model of a two-channel TI-ADC as shown in Fig. 4.1

Since the channels of a TI-ADC are designed to match as well as possible and economically viable. Therefore, all channel frequency responses should have the same characteristics but will differ due to component mismatches caused by process variations, temperature changes, and aging. Hence, we do not exactly know the channel frequency responses of a TI-ADC design, but can assume that all the channels of different TI-ADCs from the same design will share the same frequency characteristic. Therefore, similar

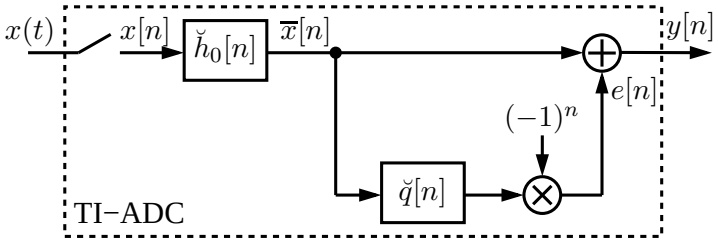

Figure 4.1: *Discrete-time system model of a two-channel TI-ADC.*

to the approach in [75] it seems reasonable to represent the normalized frequency response $\breve{Q}(e^{j\omega})$ by a polynomial series of fixed order, and to characterize the mismatches by different coefficients of this series.

For sufficiently large P, the discrete-time frequency response $\breve{Q}(e^{j\omega})$ can be represented as a P-th order polynomial, i.e.,

$$\breve{Q}(e^{j\omega}) \;=\; \sum_{p=0}^{P} \breve{c}_p D_p(e^{j\omega}), \tag{4.2}$$

where $\breve{c}_p$ is the pth coefficient of the polynomial series and

$$D_p(e^{j\omega}) = (j\omega)^p \text{ for } -\pi < \omega \leq \pi \tag{4.3}$$

is the discrete-time representation of a bandlimited continuous-time P-th order differentiator. To relate the polynomial representation of the filter with our time-domain model, we need the inverse DTFT of (4.2), which is

$$\breve{q}[n] \;=\; \sum_{p=0}^{P} \breve{c}_p d_p[n], \tag{4.4}$$

where $d_p[n]$ is the inverse DTFT of $D_p(e^{j\omega})$.

Substituting (4.4) in (4.1) gives

$$e[n] = \sum_{p=0}^{P} \breve{c}_p d_p[n] * \bar{x}[n](-1)^n \tag{4.5}$$

which can be expressed in a more concise way by using vector notation as

$$e[n] \;=\; \mathbf{c}^T \mathbf{x}_d[n], \tag{4.6}$$

where the coefficients vector is

$$\mathbf{c} \;=\; \left[\breve{c}_0, \ldots, \breve{c}_p, \ldots, \breve{c}_P\right]^T \tag{4.7}$$

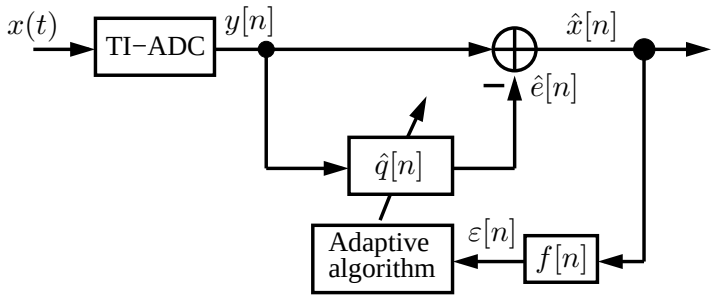

Figure 4.2: *Calibration of frequency response mismatches.*

and the signal vector is

$$\mathbf{x}_d[n] \quad = \quad \Big[x_0[n], \ldots, x_p[n], \ldots, x_P[n]\Big]^T \tag{4.8}$$

with

$$x_p[n] = d_p[n] * \bar{x}[n](-1)^n \tag{4.9}$$

and $[.]^T$ denotes the transpose. We can conclude that for a given order P the coefficients $\breve{c}_p$ in (4.7) characterize the mismatch between the two channels in a TI-ADC. To compensate the mismatches we have to identify those coefficients.

4.3 Adaptive Blind Calibration

In this section we present a blind calibration method to calibrate frequency response mismatches. For this purpose, we exploit the system model including the polynomial representation of the normalized frequency response mismatches and some slight oversampling of the input signal.

4.3.1 Calibration Principle

In Fig. 4.2 the principle of the calibration method is shown. On the left we see a TI-ADC producing the distorted output signal $y[n]$ given by (2.38), and on the right we have the calibration structure for compensating the distortions in $y[n]$. It has been shown in [71] that this structure can significantly improve the output signal $y[n]$ by using the normalized filter $\breve{Q}(e^{j\omega})$ defined in (2.27). It was, however, not shown how to find the frequency response of this filter blindly without employing a training signal. In the following we introduce a blind background calibration method that uses the FxLMS

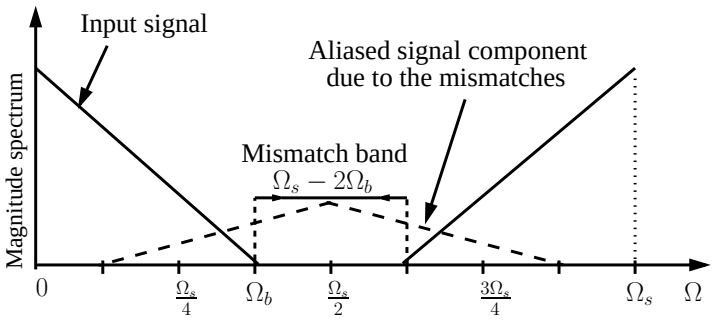

Figure 4.3: *As long as there are uncorrected mismatches, the mismatch band contains signal energy.*

algorithm [81, 82] to estimate the normalized frequency response $\breve{Q}(e^{j\omega})$ as shown in Fig. 4.2.

Firstly, in order to estimate the normalized frequency response $\breve{Q}(e^{j\omega})$, we represent the response by a polynomial as in (4.4). Secondly, we exploit oversampling as we did for the identification of gain and timing mismatches in Chapter 3, to obtain a mismatch band in the output spectrum, where in the ideal case no signal energy is present, unless there are mismatches. Since we only consider a two-channel TI-ADC, there will be only one aliasing component as illustrated in Fig. 4.3. Thirdly, we use a high-pass filter $f[n]$ to spectrally separate parts of the error signal $e[n]$ from the output signal $y[n]$, and, in a final step, we minimize the filtered error energy $\epsilon[n]$ by finding estimates $\hat{c}_p$ of the coefficients $\breve{c}_p$.

4.3.2 Calibration Structure

For the calibration we exploit the structure shown in Fig. 3.4. The structure duplicates the polynomial filter representation we used for the TI-ADC model where the time-varying filter coefficients

$$\hat{\mathbf{c}}[n] = \Big[\hat{c}_0[n], \ldots, \hat{c}_p[n], \ldots, \hat{c}_P[n]\Big]^T \tag{4.10}$$

of the calibration structure have to be identified.

As shown in Fig. 4.4, the reconstructed input signal $\hat{x}[n]$ is the difference of the TI-ADC output $y[n]$ and estimated error signal $\hat{e}[n]$ which results with (2.38) in

$$\hat{x}[n] \;\; = \;\; \bar{x}[n] + e[n] - \hat{e}[n]. \tag{4.11}$$

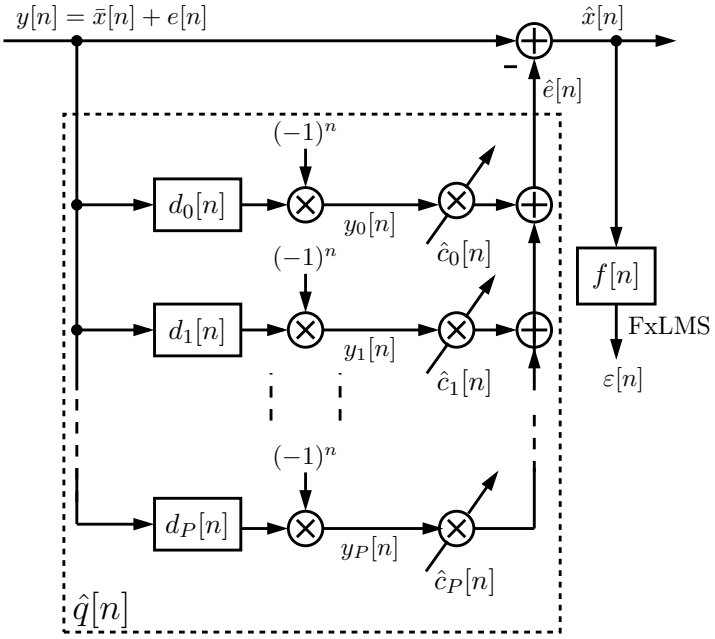

Figure 4.4: *Calibration structure.*

The estimated error $\hat{e}[n]$ is the result of adding up the weighted outputs of the P branches in Fig. 3.4, which is

$$\hat{e}[n] \quad = \quad \hat{\mathbf{c}}[n]^T \mathbf{y}_d[n], \tag{4.12}$$

where

$$\mathbf{y}_d[n] \quad = \quad \Big[y_0[n], \ldots, y_p[n], \ldots, y_P[n] \Big]^T \tag{4.13}$$

and

$$y_p[n] = d_p[n] * y[n](-1)^n \tag{4.14}$$

is the p-times differentiated and modulated input signal $y[n]$. Inserting (4.12) and (4.6) in (4.11) gives

$$\hat{x}[n] \quad = \quad \bar{x}[n] + \mathbf{c}^T \mathbf{x}_d[n] - \hat{\mathbf{c}}[n]^T \mathbf{y}_d[n]. \tag{4.15}$$

We can rewrite $\mathbf{y}_d[n]$ in (4.15) by using (2.38) and (4.8) as

$$\mathbf{y}_d[n] \quad = \quad \mathbf{x}_d[n] + \mathbf{e}_d[n], \tag{4.16}$$

where

$$\mathbf{e}_d[n] \quad = \quad \Big[e_0[n], \ldots, e_p[n], \ldots, e_P[n]\Big]^T \tag{4.17}$$

and

$$e_p[n] = d_p[n] * e[n](-1)^n. \tag{4.18}$$

Substituting (4.16) in (4.15) and rearranging gives

$$\hat{x}[n] \quad = \quad \bar{x}[n] + (\mathbf{c} - \hat{\mathbf{c}}[n])^T \mathbf{x}_d[n] - \hat{\mathbf{c}}[n]^T \mathbf{e}_d[n] \tag{4.19}$$

which explicitly shows that if the estimated coefficients vector $\hat{\mathbf{c}}[n]$ equals the actual coefficients vector $\mathbf{c}$, i.e., $\hat{\mathbf{c}}[n] = \mathbf{c}$, the reconstructed output becomes

$$\hat{x}[n] \quad = \quad \bar{x}[n] - \hat{\mathbf{c}}[n]^T \mathbf{e}_d[n], \tag{4.20}$$

where $\hat{\mathbf{c}}[n]^T \mathbf{e}_d[n]$ is the remaining error signal after reconstruction. As it has been shown in [71] the energy of the remaining error signal is much smaller than the energy of the mismatch error signal $e[n]$, whereby the signal $\hat{x}[n]$ is a much better approximation of $\bar{x}[n]$ as $y[n]$.

4.3.3 Coefficient Adaptation

After introducing the calibration structure, we have to formally relate the minimization of the error $\varepsilon[n]$ with the identification of the coefficients $\hat{\mathbf{c}}[n]$ of the calibration structure. The filtered error $\varepsilon[n]$ is given by

$$\varepsilon[n] \quad = \quad \hat{x}[n] * f[n]. \tag{4.21}$$

where $f[n]$ is a high-pass filter that spectrally separates the desired signal $\overline{x}[n]$ from the error signal $e[n]$ by attenuating $\overline{x}[n]$. Assuming that the adaptation rate of the coefficients $\hat{\mathbf{c}}[n]$ is slow enough, we can interchange the filter $f[n]$ and the time-varying coefficients $\hat{\mathbf{c}}[n]$ [81], which leads with (4.15) and (4.21) to

$$\varepsilon[n] \quad = \quad \mathbf{c}^T \left(\mathbf{y}_d^f[n] - \mathbf{e}_d^f[n]\right) - \hat{\mathbf{c}}[n]^T \mathbf{y}_d^f[n] \tag{4.22}$$

where $\bar{x}[n]$ is removed by the filter $f[n]$ and

$$\mathbf{y}_d^f[n] \quad = \quad \mathbf{x}_d^f[n] + \mathbf{e}_d^f[n]. \tag{4.23}$$

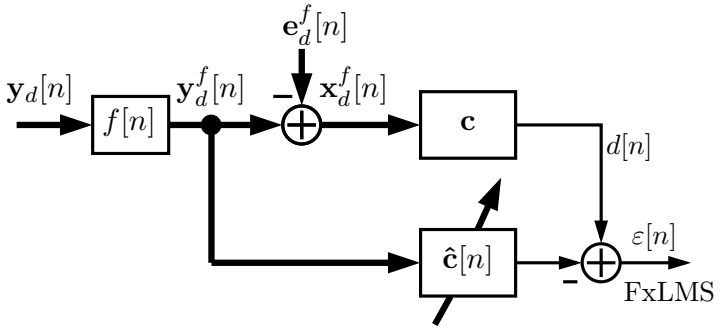

Figure 4.5: *Model of the identification structure illustrating the identification of* $\hat{\mathbf{c}}[n]$ *coefficients.*

with

$$\mathbf{x}_d^f[n] \quad = \quad [x_0[n] * f[n], \ldots, x_p[n] * f[n], \ldots, x_P[n] * f[n]]^T \tag{4.24}$$

and

$$\mathbf{e}_d^f[n] = [[e_0[n] * f[n], \ldots, e_p[n] * f[n], \ldots, e_P[n] * f[n]]^T \,. \tag{4.25}$$

With (4.22)-(4.23) we have a classical identification problem illustrated in Fig. 4.5 that can be solved by using the FxLMS algorithm [81, 82] as

$$\hat{\mathbf{c}}[n] \quad = \quad \hat{\mathbf{c}}[n-1] + \mu \cdot \varepsilon[n] \cdot \mathbf{y}_d^f[n] \tag{4.26}$$

where μ is the step-size parameter.

4.3.4 Performance Analysis

In analyzing the identification performance of (4.22), we resort to the classical stochastic minimum-mean square analysis [81] of the FxLMS algorithm given in (4.26). The error of the structure can be written as

$$\varepsilon[n] \quad = \quad \mathbf{c}^T \left(\mathbf{y}_d^f[n] - \mathbf{e}_d^f[n] \right) - \hat{\mathbf{c}}[n]^T \mathbf{y}_d^f[n]. \tag{4.27}$$

where the term $\mathbf{c}^T(\mathbf{y}_d^f[n] - \mathbf{e}_d^f[n])$ represents the desired signal and $\mathbf{y}_d^f[n]$ is the input signal to the adaptive filter. Therefore, the adaptive filter is driven by an additional signal component $\mathbf{e}_d^f[n]$ that will lead to a certain bias in the MMSE solution. For the

derivation of the MMSE solution we assume that $\mathbf{x}_d^f[n]$ and $\mathbf{e}_d^f[n]$ are uncorrelated, which can be justified by the fact that LMS based algorithms rather use averages of the time series than using ensemble averages, where the time-averaged cross-correlation between $\mathbf{x}_d^f[n]$ and $\mathbf{e}_d^f[n]$ will tend to zero. Using this assumption we can derive the estimated coefficient vector as [81]

$$\hat{\mathbf{c}}[n] = \left(\mathbf{R}_{\mathbf{y}_d^f\mathbf{y}_d^f}\right)^{-1}\mathbf{p} \tag{4.28}$$

where $\mathbf{R}_{\mathbf{y_d^f y_d^f}}$ is the autocorrelation matrix of $\mathbf{y}_d^f[n]$, i.e.,

$$\mathbf{R}_{\mathbf{y_d^f y_d^f}} = E\{\mathbf{y}_d^f[n]\mathbf{y}_d^f[n]\} \tag{4.29}$$

and $\mathbf{p}$ is the cross-correlation vector given by

$$\begin{aligned}\mathbf{p} &= E\{\mathbf{c}^T\left(\mathbf{y}_d^f[n]-\mathbf{e}_d^f[n]\right)\mathbf{y}_d^f[n]\}\\ &= \left(\mathbf{R}_{\mathbf{y}_d^f\mathbf{y}_d^f}-\mathbf{R}_{\mathbf{e}_d^f\mathbf{e}_d^f}\right)\mathbf{c}\end{aligned} \tag{4.30}$$

Substituting (4.29) and (4.30) in (4.28) results in

$$\hat{\mathbf{c}}[n] = \left(\mathbf{I}-(\mathbf{R}_{\mathbf{y}_d^f\mathbf{y}_d^f})^{-1}\mathbf{R}_{\mathbf{e}_d^f\mathbf{e}_d^f}\right)\mathbf{c} \tag{4.31}$$

where the auto-correlation matrix $\mathbf{R}_{\mathbf{e}_d^f\mathbf{e}_d^f}$ of the signal $\mathbf{e}_d^f[n]$ causes a bias in the estimate. However, since the energy of the signal $\mathbf{x}_d^f$ is several orders of magnitude larger than the energy of the signal $\mathbf{e}_d^f$, the bias has only a minor influence on the overall performance of the calibration structure.

4.4 Simulation Results

In this section we present the simulation results for the proposed blind calibration structure to characterize its performance. The overall performance of the blind calibration structure was evaluated by the signal-to-noise ratio (SNR). The SNR before calibration was evaluated as

$$\mathrm{SNR} = 10\log_{10}\left(\frac{\sum_{n=0}^{N-1}|\bar{x}[n]|^2}{\sum_{n=0}^{N-1}|\bar{x}[n]-y[n]|^2}\right) \tag{4.32}$$

and after calibration as

$$\mathrm{SNR} = 10\log_{10}\left(\frac{\sum_{n=0}^{N_1-1}|\bar{x}[n]|^2}{\sum_{n=0}^{N_1-1}|\bar{x}[n]-\hat{x}[n]|^2}\right), \tag{4.33}$$

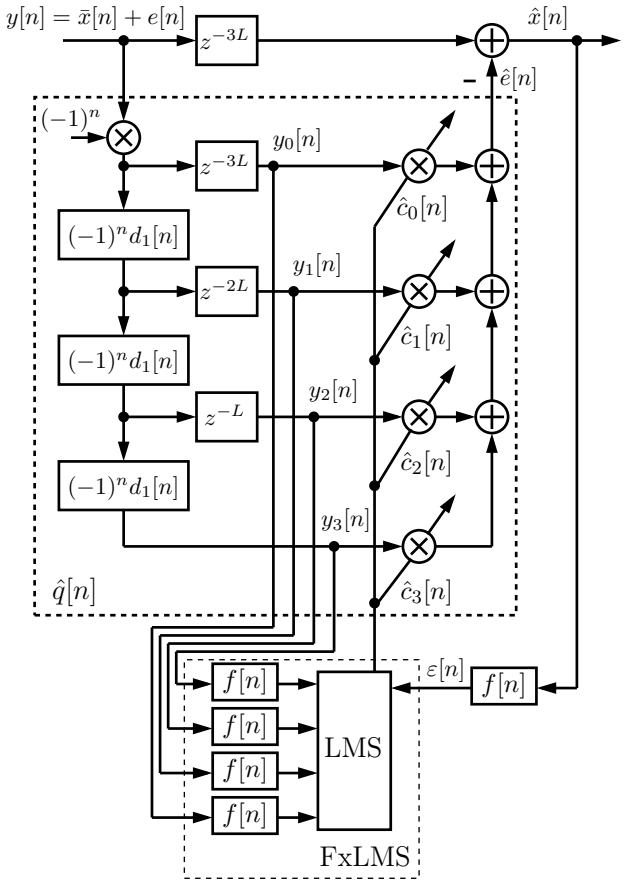

Figure 4.6: *Implementation example of the blind calibration structure for $P = 3$.*

where N denotes the number of samples used to calculate the SNR before calibration and N_1 denotes the number of samples used to calculate the SNR after calibration (once the FxLMS algorithm has converged). For all simulations, we used an input signal bandlimited to $\Omega_b T_s = 0.8\pi$, from which we took 2^{22} samples according to the presented mismatch model.

4.4.1 Implementation of the Calibration Structure

A possible implementation of the blind calibration structure for $P = 3$ as it was used for the simulations is shown in Fig. 4.6. The complexity of the structure is reduced by some minor modifications. By shifting the modulators $(-1)^n$ to the start of the blind calibration structure, they can be combined into a single modulator. To maintain the

same output signals as before, the coefficients of the differentiators have to be modulated as well. Additionally, we have cascaded differentiators of first order $d_1[n]$ to obtain higher order differentiators. The order of the differentiator $d_1[n]$ was 40, and it was designed using the MATLAB function 'firpm'. The high-pass filter $f[n]$ was designed using MATLAB filter design tool 'fdatool'. The number of taps of $f[n]$ were 41 and its magnitude response is shown in Fig. 4.7. Ideally, the signal $\mathbf{y}_d^f[n]$ is the filtered version

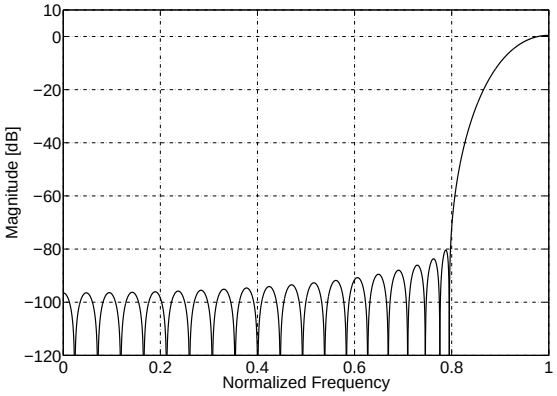

Figure 4.7: *Magnitude response of the high-pass filter $f[n]$ used in Example 1 with order 40 and a starting passband frequency at 0.8π.*

of the signal vector $\mathbf{y}_d[n]$, but as we will show in the simulation for gain and timing mismatches, we can also use a much simpler update equation

$$\hat{\mathbf{c}}[n] \quad = \quad \hat{\mathbf{c}}[n-1] + \mu \cdot \varepsilon[n] \cdot \mathbf{y}_d[n-K] \tag{4.34}$$

where K is the delay of the linear-phase high-pass filter $f[n]$. Hence, a delayed version instead of a filtered version is used. This reduces the implementation complexity considerable, as we only need a single high-pass filter, but, as drawback, the convergence time increases.

The following examples describe the simulation results using different types of mismatch models and input signals. In all of these examples, the choice of step size parameter μ was based on the experimentation, however, it never exceeded the stability bounds of FxLMS algorithm as defined in [81, 82].

4.4.2 Calibration of Frequency Response Mismatches: White Gaussian Noise Input Signal

First, we considered a white-Gaussian noise (WGN) input signal bandlimited to $\Omega_b T_s \leq 0.8\pi$ and with zero-mean and variance $\sigma^2 = 1$. The step-size μ was 0.5 whereas the coefficients vector $\mathbf{c}$ was taken randomly as

$$\mathbf{c} = [-0.025, 0.005, -0.0015, -0.0001]. \tag{4.35}$$

Figure 4.8 shows the power spectrum of the uncompensated TI-ADC output $y[n]$. The SNR according to (4.32) was 32.6 dB. The power spectrum of the reconstructed input signal $\hat{x}[n]$, once the FxLMS algorithm has converged (approximately after 4×10^5), is shown in Fig. 4.9, where the SNR according to (4.33) was 60.3 dB. This was an improvement of 27.7 dB and equals the result one would obtain by directly using the coefficient vector $\mathbf{c}$ and the first stage of the calibration structure presented in [71]. The convergence behavior of the estimated coefficients is shown in Fig. 4.10. The estimated coefficients settle nicely to the optimum coefficient values.

4.4.3 Calibration of Frequency Response Mismatches: Multitone Input Signal

Next we considered a multitone input signal consisting of 42 sinusoids bandlimited to 0.8π and having a constant amplitude, uniformly spaced frequencies, and random phases. Moreover, the signal was quantized to 16 bits where the quantization step size was given by $2/(2^{16} - 1)$. The channel frequency responses were taken as in [75], i.e.,

$$\hat{H}_m(j\Omega) = \frac{1}{1 + j\frac{\Omega}{\Omega_c}(1 + \Delta_m)} e^{j\Omega T r_m} \tag{4.36}$$

where Ω_c is the 3-dB cutoff frequency of the first order filter, r_m are the relative timing offsets and Δ_m are the deviations from Ω_c. The cutoff frequency was taken equal to the sampling frequency i.e. $\Omega_c = \Omega_s$. The step-size parameter μ was chosen as 0.09 while the values of r_m were $[-0.02, +0.02]$ and of Δ_m were $[-0.005, +0.005]$ similar to the setting in [75], but for a two-channel TI-ADC. The power spectrum of the uncalibrated output $y[n]$ is shown in Fig. 4.11. The calculated SNR was 31.1 dB. The power spectrum of the reconstructed input signal $\hat{x}[n]$ using a 2nd order calibration structure ($P = 2$) is shown in Fig. 4.12. The calculated value of the SNR, once FxLMS algorithm has converged, was 62.6 dB; thus doubling the initial SNR. By using the multitone signal we can explicitly recognize that not only the energy in the mismatch band is reduced considerably but also the energy of the aliasing components that are overlapping with the input signal spectra has been minimized.

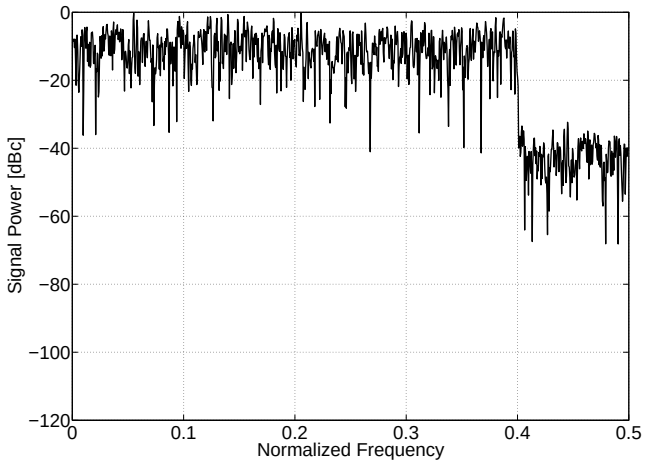

Figure 4.8: *Power spectrum of the uncalibrated output $y[n]$ for a white Gaussian noise (WGN) input signal. The SNR is* 32.6 *dB.*

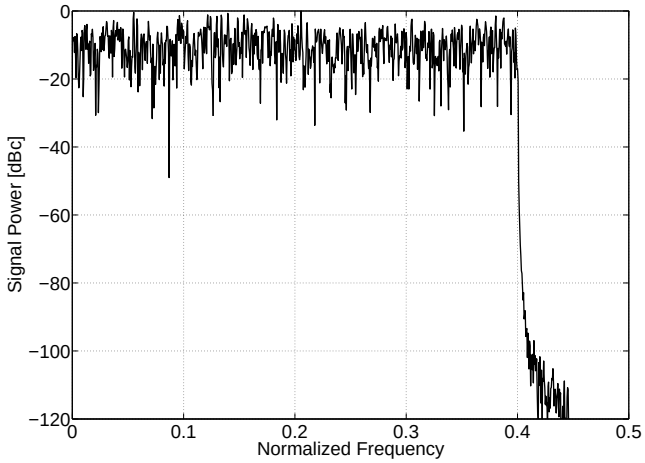

Figure 4.9: *Power spectrum of the reconstructed WGN input signal $\hat{x}[n]$. The SNR after calibration is* 60.3 *dB, which is an improvement of* 27.7 *dB.*

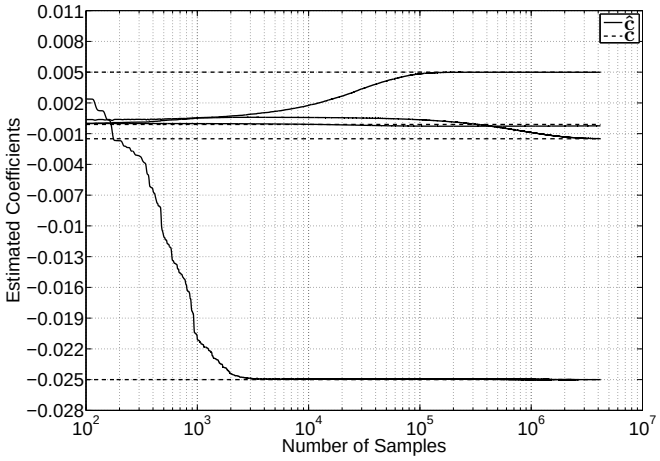

Figure 4.10: *Convergence behavior of the estimated coefficients* $\hat{c}_0[n]$, $\hat{c}_1[n]$, $\hat{c}_2[n]$, *and* $\hat{c}_3[n]$ *(solid lines) for the case of a WGN input signal. For a step-size of* $\mu = 0.5$, *the estimated coefficients are converging well towards the given coefficient values (dashed lines).*

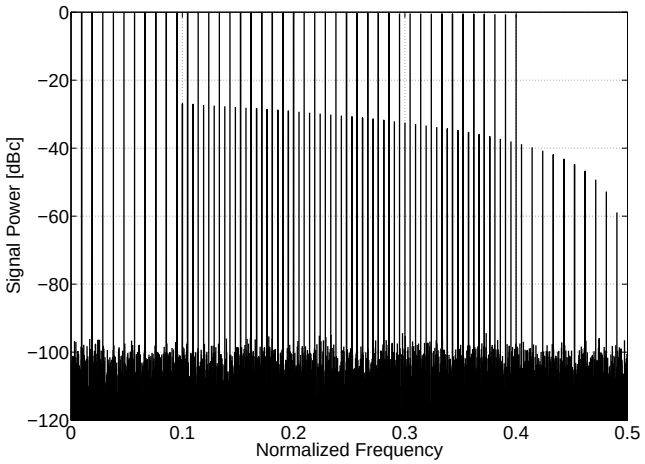

Figure 4.11: *Power spectrum of the uncalibrated output* $y[n]$. *The input was a multitone signal composed of* 42 *sinusoids and bandlimited to* 0.8π. *The SNR is* 31.1 *dB.*

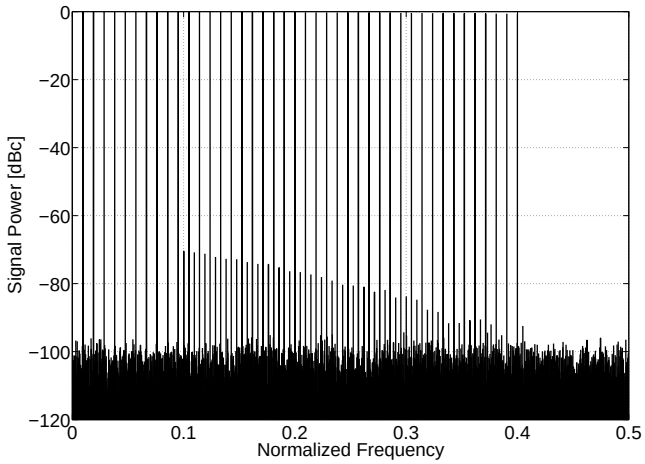

Figure 4.12: *Power spectrum of the reconstructed input signal* $\hat{x}[n]$ *after using a* 2*nd order calibration structure. The SNR after calibration is* 62.6 *dB, which was an improvement of* 31.5 *dB,*

4.4.4 Calibration of Bandwidth Mismatches: Multitone Input Signal

In this example we demonstrate the calibration of bandwidth mismatches as modeled in [64, 66]. We again used a multitone input signal with 42 sinusoids bandlimited to 0.8π and had a constant amplitude, uniformly spaced frequencies, and random phases.

According to [64, 66], the channel frequency responses are given for a two-channel TI-ADC as

$$\hat{H}_m(j\Omega) = \frac{1}{1 + j\frac{\Omega}{(1+\Delta_m)\Omega_c}} \frac{1 - e^{-(1+\Delta_m)\Omega_c T} e^{-j\Omega T}}{1 - e^{-(1+\Delta_m)\Omega_c T} e^{-j2\Omega T}} \tag{4.37}$$

where Ω_c is the 3-dB cutoff frequency of each sample-and-hold of the individual channel ADCs, and Δ_m are the deviations from Ω_c, i.e., bandwidth mismatches. For this simulation, we assume a cutoff frequency of $\Omega_c = 3/2\Omega_s$ with mismatch values given in Tab. 4.1, and used a step-size of $\mu = 0.03$ for the FxLMS algorithm. In Tab. 4.2 the initial SNR and the SNR after calibration is given for the different mismatch values and for different orders P of the polynomial series. From Tab. 4.2 we see that for increasing order we obtain better SNRs after calibration as the mismatch model is represented more accurately. The power spectra for the uncalibrated output $y[n]$ and the reconstructed input $\hat{x}[n]$ for the case of 5% bandwidth mismatch are shown in Fig. 4.13 and 4.14, respectively.

Table 4.1: *Simulated bandwidth mismatch values.*

Mismatch	Δ_1	Δ_2
2%	0.99	1.01
5%	0.98	1.03
10%	0.95	1.05

Table 4.2: *Initial and final SNR for bandwidth mismatch values from Tab. 4.1 and for different orders of the calibration structure.*

		Final SNRs		
Mismatch	Initial SNR	$P = 1$	$P = 2$	$P = 3$
2%	56.4 dB	70 dB	80.1 dB	84.3 dB
5%	48.5 dB	62.1 dB	72.5 dB	75.6 dB
10%	42.4 dB	56 dB	66 dB	70 dB

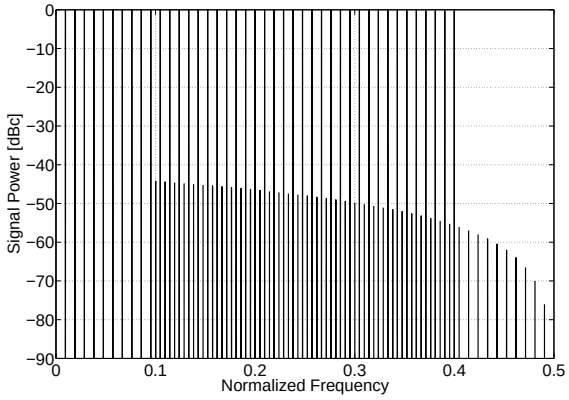

Figure 4.13: *Power spectrum of the output $y[n]$ with 5% bandwidth mismatches. The SNR is 48.5 dB.*

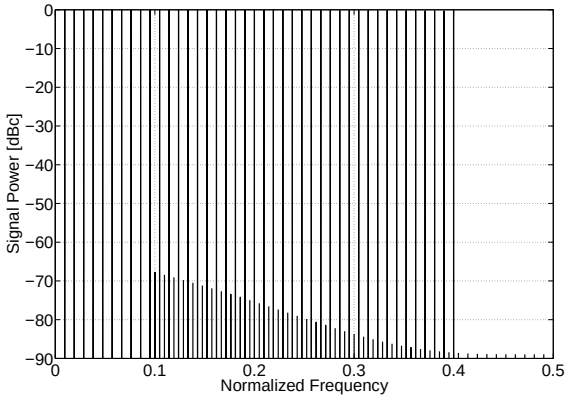

Figure 4.14: *Power spectrum of the reconstructed output $\hat{x}[n]$ for the case of bandwidth mismatch calibration. For a 3rd order calibration structure and the SNR after calibration is 75.6 dB, which is an improvement of 27.1 dB.*

4.4.5 Calibration of Gain and Timing Mismatches: White Gaussian Noise Input Signal

In this example we considered a WGN input signal bandlimited to 0.8π and having zero mean and variance $\sigma^2 = 1$. By modeling the channel frequency responses as

$$\hat{H}_m(j\Omega) = g_m e^{j\Omega T r_m} \tag{4.38}$$

where g_m and r_m are the relative gain mismatches and timing offsets, respectively. The calibration of gain and timing mismatches for an M-channel TI-ADC has been demonstrated in Chapter 3, however this example uses only a two-channel TI-ADC and it further demonstrates the difference in the convergence time for the filtered and delayed versions of LMS algorithm given by (4.26) and (4.34) respectively.

The simulated values were $[1, 1.01]$ for g_m and $[0, -0.02]$ for r_m as given in [12]. For the given gain and timing mismatches, the coefficient vector $\mathbf{c}$ can be sufficiently closely approximated by using a first order truncated Taylor's series, which gives

$$\mathbf{c} = [-0.00498, 0.01]. \tag{4.39}$$

Figures 4.15 and 4.16 show the power spectra of the uncalibrated output $y[n]$ and reconstructed output $\hat{x}[n]$, respectively. For the uncalibrated signal the SNR was 36.3 dB, and, for the reconstructed output signal with a step size of $\mu = 0.06$, the SNR was 72.8 dB, i.e., an improvement of 36.5 dB. Figures 4.17 and 4.18 show the convergence

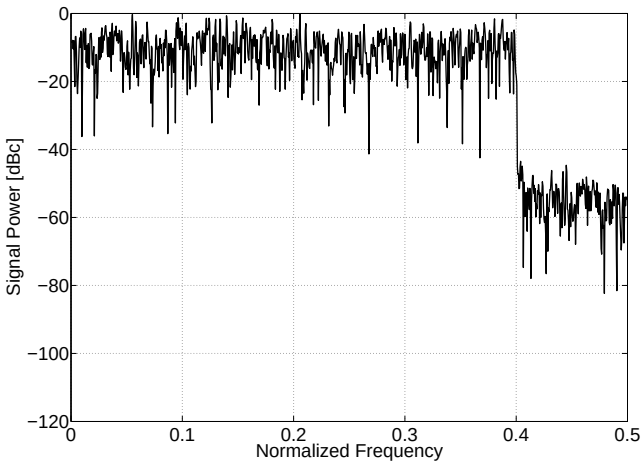

Figure 4.15: *Power spectrum of the uncalibrated output $y[n]$ with gain and timing mismatches. The SNR is* 36.3 *dB.*

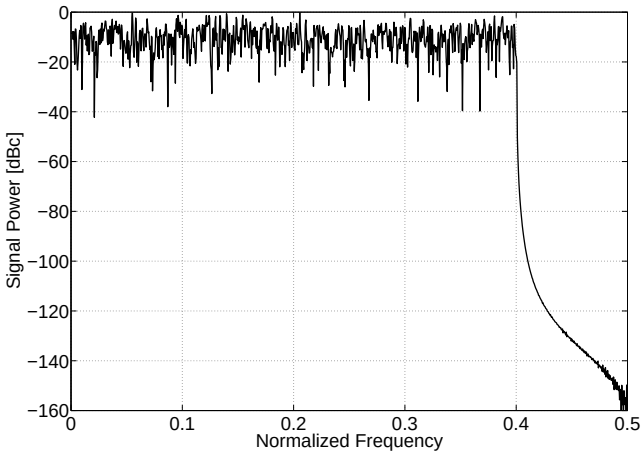

Figure 4.16: *Power spectrum of the reconstructed output $\hat{x}[n]$ using a* 1*st order calibration structure. The SNR is* 72.8 *dB which is an improvement of* 36.5 *dB.*

of the estimated gain and timing mismatches. It can be seen that the filtered version of LMS given by (4.26) converges faster than as compared to the delayed version given by (4.34). This behavior supports the usage of extra high-pass filters to speed up the convergence rate in the implementation structure shown in Fig. 4.6.

4.5 Conclusions

In this chapter we have presented a blind calibration structure to calibrate frequency response mismatches in a two-channel TI-ADC. We have presented the system model of a two-channel TI-ADC with frequency response mismatches. Later this system model has been approximated by a P-th order polynomial resulting in approximate expressions for the error signals. Based on the approximate system model we have developed the blind calibration structure that uses the FxLMS algorithm to identify the unknown coefficients of the polynomials and thus compensates the frequency response mismatches. We have demonstrated the flexibility of the blind calibration structure by calibrating not only the frequency response mismatches but also the gain, timing, and bandwidth mismatches by using when multitone and WGN input signals. The simulation results have confirmed that we can achieve a considerable amount of improvement in the SNR after calibration. Furthermore, the structure is easily scalable for higher-order polynomial approximations where each increase in the polynomial-order requires one additional differentiator, one time-varying multiplier, and one adder. However, the straight forward extension to more than two channels works well for gain and timing mismatches, and, therefore, is an open research question for general frequency response mismatches.

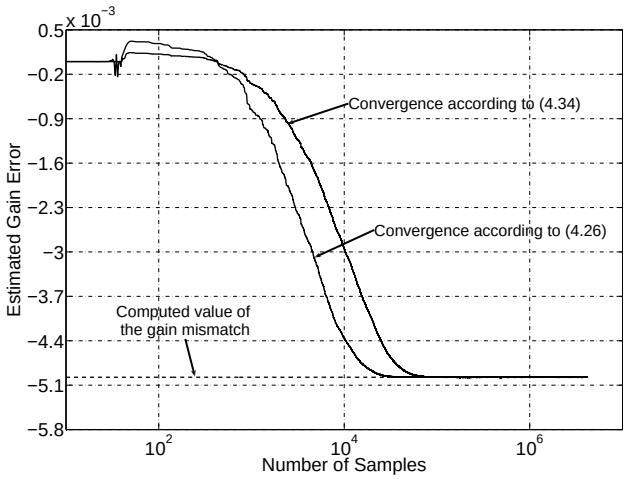

Figure 4.17: *Convergence behavior of the estimated gain mismatch coefficients according to (4.26) and (4.34).*

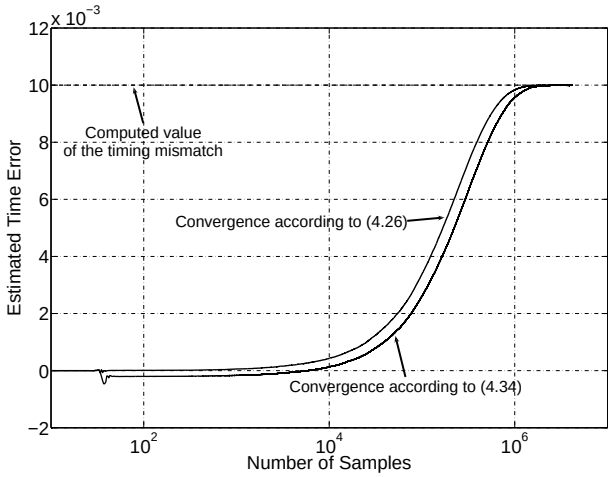

Figure 4.18: *Convergence behavior of the estimated relative timing offsets coefficients according to (4.26) and (4.34).*

5

Adaptive Non-Blind Background Calibration of Frequency Response Mismatches

This chapter[1] investigates the non-blind background calibration of frequency response mismatches in an M-channel TI-ADC. The non-blind calibration structure comprises an M-periodic time-varying compensation filter. The coefficients of the time-varying filter are estimated by using an M-periodic LMS algorithm. The introduced calibration structure may be used to calibrate any linear frequency response mismatches.

After the introduction in Section 5.1 we analyze the cascade of an M-channel TI-ADC with an M-periodic time-varying filter in Section 5.2. The coefficient sets of the compensation filter are determined adaptively by using an additional low-resolution ADC as reference to an M-periodic LMS algorithm as described in Section 5.3. The simulation results are presented in Section 5.4 to characterize the performance of the proposed adaptive non-blind compensation structure. Finally the chapter is concluded in Section 5.5.

5.1 Introduction

As discussed in Chapter 2, a TI-ADC can be modeled as an M-periodic time-varying system, where for each time instant we get a different response of the M-channel TI-ADC. Such a behavior is usually caused by fabrication errors, temperature variations, and aging effects. In such a scenario, the calibration of frequency response mismatches requires an appropriate discrete-time M-periodic time-varying filter. Such a filter is characterized by M time-invariant impulse responses or M coefficient sets. Whenever the behavior of the TI-ADC changes, these coefficient sets need to be recomputed. The

[1] Parts of this chapter have been published in [18]

computation of the coefficient sets either can be performed adaptively or in a non-adaptive fashion such as using a least-squares design. In both cases, a reference is needed to compute the underlying coefficients sets. The reference can be the ideal input signal itself or can be an estimated or measured version of it. For a typical calibration scenario, we usually do not have any access to the ideal input signal, hence such a choice of reference seems unrealistic. However, an additional low-resolution ADC can be employed that operates at the sampling rate of the corresponding M-channel TI-ADC to obtain a measured version of the input signal. The TI-ADC and the low-resolution ADC are operated by the same input signal. An immediate issue that arises in this scenario is the increased power consumption due to the usage of an additional ADC. Since the power consumption of an ADC is directly proportional to its resolution, a low-resolution ADC does not significantly increase power consumption of a TI-ADC. For example, compared to the power dissipation of 33 mW for a 10-bit 100MS/s pipeline converter a 4-bit 1.25GS/s flash converter has a power dissipation of only 2.5 mW [87]. Furthermore, technology scaling has also helped to improve the power efficiency of low-resolution ADCs over time. On average, the power dissipation for flash and pipeline ADCs has halved every 2.5 years over the past ten years [87].

The use of an M-periodic time-varying filter to compensate frequency response mismatches in an M-channel TI-ADC has been earlier investigated in [71–73, 88]. A least-squares filter design method for frequency response mismatches is presented in [72]. It is an extension to the work presented in [89] and has a reduced filter design complexity compared to [67], but the complexity is still demanding and the method requires known frequency responses or special input signals to identify them. The same could be said about the filter design method using multi-channel filters introduced in [88]. To simplify the identification task, the authors investigated the special case of bandwidth mismatches. An adaptive technique utilizing an M-periodic time-varying feedforward equalizer to correct gain, timing, and bandwidth mismatches is shown in [73]. Basically, the method uses the decoded symbols to generate a reference signal on sampling rate for the mismatch calibration, which is a non-trivial task. In [71] a flexible and scalable structure to compensate frequency response mismatches in a TI-ADC has been presented. The authors have used the output of the TI-ADC as a reference to determine M impulse responses of the time-varying compensation filter. But in this regard they need to know the average frequency response of the TI-ADC. This average frequency response was determined by using sinusoidal test signals. Moreover, the authors have demonstrated the flexibility of their time-varying compensation structure by compensating also the bandwidth, and time-offset mismatches beside the frequency response

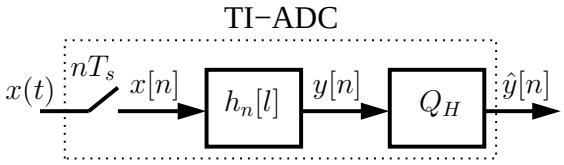

Figure 5.1: *Time-varying system model of a high-resolution TI-ADC with a quantizer Q_H.*

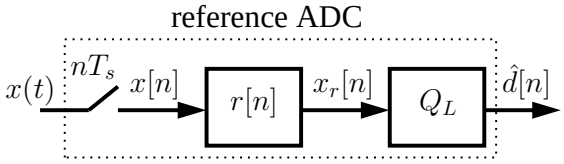

Figure 5.2: *A low-resolution ADC with an impulse response $r[n]$ and quantizer Q_L.*

mismatches. Such a flexibility has earlier been demonstrated in Chapter 4 of this dissertation for the frequency response model of a two-channel TI-ADC represented by polynomials.

We start with the time-varying system model of a TI-ADC introduced in Section 2.4 but here we explicitly include a quantizer Q_H that yields the output $\hat{y}[n]$, i.e.,

$$y[n] = \sum_{l=0}^{\infty} h_n[l]x[n-l] \quad \text{and} \quad \hat{y}[n] = Q_H(y[n]). \tag{5.1}$$

The resulting system is shown in Fig. 5.1.

The output $\hat{y}[n]$ is passed to an M-periodic time-varying calibration filter $g_n[l]$. To obtain the coefficients sets of $g_n[l]$, we need a reference. For this purpose we use the output of an additional low-resolution ADC with an impulse response $r[n]$ followed by a quantizer Q_L, as shown in Fig. 5.2. The output $\hat{d}[n]$ of the low-resolution ADC can be written as

$$x_r[n] = \sum_{l=0}^{+\infty} r[l]x[n-l] \quad \text{and} \quad \hat{d}[n] = Q_L(x_r[n]) \tag{5.2}$$

This output acts as reference for an M-periodic LMS algorithm that computes the coefficient sets of $g_n[l]$. Hence the adaptive calibration technique presented in this chapter and in [73] are similar but obtain their reference signals in different ways. Finally, the output of $g_n[l]$ is the frequency response mismatch calibrated output $y_c[n]$.

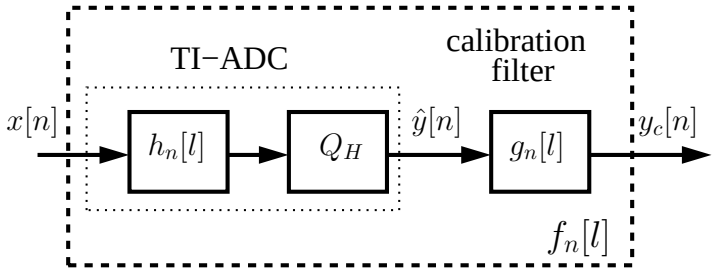

Figure 5.3: *Cascade of the two M-periodic time-varying filters $h_n[l]$ and $g_n[l]$ results in a new time-varying filter $f_n[l]$.*

5.2 Cascaded Time-Varying Filters

Since the output $\hat{y}[n]$ of the TI-ADC acts as input to the M-periodic time-varying compensation filter $g_n[l]$, which is thus cascaded with the M-periodic time-varying filter $h_n[l]$. This cascading of the two M-periodic time-varying filters results in a new M-periodic time-varying filter $f_n[l]$ as shown in Fig. 5.3. Next we present a detailed analysis to get an analytic representation for $f_n[l]$.

Analysis

Using (5.1) we can rewrite the output $\hat{y}[n]$ of the TI-ADC as

$$\hat{y}[n] = \sum_{l_1=0}^{\infty} h_n[l_1]x[n-l_1] \tag{5.3}$$

and the output of $g_n[l]$ as

$$y_c[n] = \sum_{l_2=0}^{L} g_n[l_2]\hat{y}[n-l_2], \tag{5.4}$$

where L denotes the order of $g_n[l]$.

Substituting (5.3) in (5.4) results in

$$y_c[n] = \sum_{l_2=0}^{L}\sum_{l_1=0}^{\infty} g_n[l_2]h_{n-l_2}[l_1]x[n-(l_1+l_2)]. \tag{5.5}$$

Defining

$$l = l_1 + l_2 \tag{5.6}$$

and

$$p = l_2 \tag{5.7}$$

we can rewrite (5.5) as

$$y_c[n] = \sum_{l=0}^{\infty} \sum_{p=0}^{L} g_n[p] h_{n-p}[l-p] x[n-l]. \tag{5.8}$$

which can be rewritten as

$$y_c[n] = \sum_{l=0}^{\infty} f_n[l] x[n-l] \tag{5.9}$$

with

$$f_n[l] = \sum_{p=0}^{L} g_n[p] h_{n-p}[l-p]. \tag{5.10}$$

Equation (5.10) represents the cascade of the two M-periodic time-varying filters $h_n[l]$ and $g_n[l]$ as shown in Fig. 5.3. The resulting cascaded time-varying filter $f_n[l]$ is also M-periodic i.e. $f_n[l] = f_{n+M}[l]$.

5.3 Adaptive Calibration

Based on the time-varying system model of a TI-ADC and the cascaded time-varying filters structure, we now present a calibration structure comprising a cascaded FIR filter $f_n[l]$ and an additional low-resolution ADC $d[n]$ as shown in Fig. 5.4. This structure

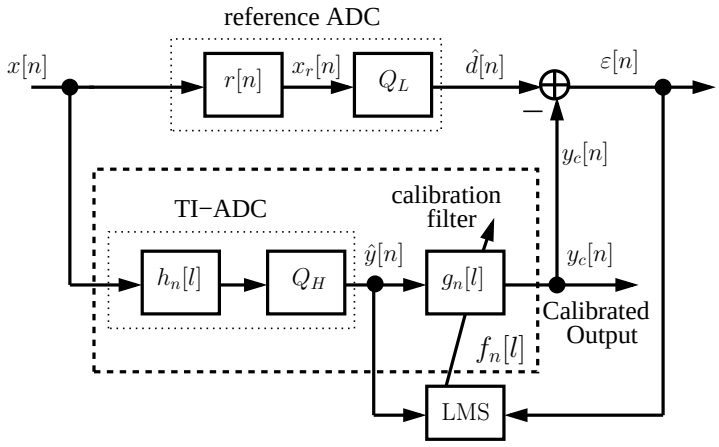

Figure 5.4: *Adaptive non-blind calibration structure comprising an M-periodic time-varying causal FIR filter $f_n[l]$ and a filter $r[n]$ representing an additional low-resolution ADC generating the desired input $\hat{d}[n]$ for the M-periodic LMS algorithm that is used to adapt the coefficient sets of $g_n[l]$ to yield the calibrated output $y_c[n]$.*

represents the typical channel equalization problem where the response of an M-channel TI-ADC, i.e., $h_n[l]$, replaces the communication channel and $g_n[l]$ is an M-periodic equalizer. The coefficient sets of $g_n[l]$ are estimated by using the M-periodic LMS algorithm.

The adaptation error $\varepsilon[n]$ is given by

$$\varepsilon[n] = \hat{d}[n] - y_c[n]. \tag{5.11}$$

Substituting $y_c[n]$ and $\hat{d}[n]$ from (5.9) and (5.2) in (5.11) and rearranging

$$\varepsilon[n] = \sum_{l=0}^{+\infty} (r[l] - f_n[l]) \cdot x[n-l]. \tag{5.12}$$

Ideally, the filter $r[n]$ is chosen in a way so that $\varepsilon[n]$ in (5.12) becomes small. In our case, $\varepsilon[n]$ is minimzed by using an M-periodic LMS algorithm as

$$\mathbf{G}_{n+M}[l] = \mathbf{G}_n[l] + \mu \cdot \mathbf{y}[n-l] \cdot \varepsilon[n], \tag{5.13}$$

where $\mathbf{G}$ is the matrix of the coefficient sets of $g_n[l]$ whereas $\hat{\mathbf{y}}[n]$ is the input vector, and μ is the adaptation step size for the M-periodic LMS algorithm. Equation (5.13) is different from a standard LMS algorithm because it updates a different coefficient set out of M sets during each iteration. Once the M-th coefficient set is updated then it starts again from the first coefficient set and continues in a round robin fashion.

5.4 Simulation Results

Simulations were performed to investigate the performance of the compensation structure with a four-channel TI-ADC suffering from frequency response mismatches. The channel frequency responses being used for the simulations were

$$\hat{H}_m(j\Omega) = \frac{\alpha_m}{1 + j\frac{\Omega}{(1+\Delta_m)\Omega_c}} e^{j\Omega T r_m} \tag{5.14}$$

where Ω^c is the 3-dB cutoff frequency, α_m are the gain mismatches, r_m are the relative timing offsets from the ideal sampling instants, and Δ_m are the relative frequency offsets from Ω_c, i.e., bandwidth mismatches. We have simulated a 16-bit four-channel TI-ADC with sampling rate $\Omega_s = \Omega_c$.

For all the examples that follow we considered a multitone input signal bandlimited to $0.8\Omega_s/2$ and having random amplitudes, frequencies, and phases. The simulated gain mismatches, relative timing, and frequency offset values are shown in Tab. 5.1. The

Table 5.1: *Simulated gain mismatches, relative timing and frequency offsets values*

ADC	α_m	r_m	Δ_m
ADC_0	1.01	$-0.007T_s$	$+0.10$
ADC_1	0.98	$+0.002T_s$	-0.02
ADC_2	0.99	$-0.003T_s$	-0.05
ADC_3	1.02	$+0.008T_s$	$+0.05$

frequency response of the low-resolution ADC was taken as the first-order frequency response given by

$$R(j\Omega) = \frac{1.03}{1 + j\frac{\Omega}{\Omega_c}}. \tag{5.15}$$

For the adaptation, the step size μ was computed as

$$\mu = \frac{2}{L\sigma_x^2 100000}, \tag{5.16}$$

where L is the order of the compensation filter $g_n[l]$ and σ_x^2 is the variance of the input signal.

The performance before compensation was measured by computing the value of the SNR as

$$\text{SNR} = 10\log_{10}\left(\frac{\sum_{n=0}^{N-1}|x_r[n]|^2}{\sum_{n=0}^{N-1}|x_r[n]-y[n]|^2}\right) \tag{5.17}$$

and after compensation was measured as

$$\text{SNR} = 10\log_{10}\left(\frac{\sum_{n=0}^{N_1-1}|x_r[n]|^2}{\sum_{n=0}^{N_1-1}|x_r[n]-y_c[n]|^2}\right), \tag{5.18}$$

where N denotes the number of samples used to calculate the SNR before calibration, N_1 denotes the number of samples used to calculate the SNR after calibration (once the M-periodic LMS algorithm has converged), and $x_r[n]$ is the convolution of $x[n]$ and $r[n]$ as shown in Fig. 5.2.

Example 1

In this example we demonstrate the performance of the compensation structure. We took $N = 2^{24}$ samples of the input signal. The values of Q_L and Q_H were 2 bits and 16 bits, respectively, while we used a compensation filter $g_n[l]$ with $L = 17$ taps.

Figure 5.5 shows the power spectrum of the uncompensated output signal $y[n]$. The SNR was 28.3 dB. The power spectrum of the compensated output signal $y_c[n]$ is shown in Fig. 5.6. The computed value of the SNR (once the M-periodic LMS algorithm has converged, i.e., for $N_1 = 4096$) was 49 dB which was an approximate improvement of 21 dB as compared to the uncompensated output.

Example 2

In this example we show the effect of the resolution of Q_L on the SNR, using different numbers of samples for a compensation filter $g_n[l]$ with 17 taps as shown in Fig. 5.7. By increasing the number of reference bits Q_L and the number of samples, the SNR increases. For $Q_L = 2$ bits, an SNR improvement up to 21 dB was observed using 2^{24} samples while for $Q_L = 6$ bits, an SNR improvement up to 28 dB was observed using 2^{24} samples.

Example 3

This example demonstrates the effect of the filter order L of $g_n[l]$ on the SNR. For this simulation we used $Q_L = 2$ bits and 2^{24} samples of the input signal. As can be seen in Fig. 5.8 that value of the SNR decreases for longer filters. This effect can be improved either by increasing the number of samples or alternatively by increasing the value of Q_L as shown in Fig 5.8. However with the increase of Q_L, convergence can be achieved with less samples while using a similar step size μ. For a filter $g_n[l]$ with 9 taps we observed an improvement of up to 22 dB in the SNR.

5.5 Conclusions

In this chapter we have presented an adaptive non-blind compensation structure to compensate the frequency response mismatches in an M-channel TI-ADC. By modeling an M-channel TI-ADC as an M-periodic time-varying system, we have used an M-periodic time-varying FIR filter for compensation. The coefficient sets of the compensation filter have been estimated by using the output of an additional low-resolution ADC as reference to an M-periodic LMS algorithm. Simulations have shown that by using a large number of samples with a reasonably smaller step size, the M-periodic LMS algorithm has well estimated the coefficient sets of the time-varying compensation filter. Furthermore we have seen that, by using a time-varying compensation filter with smaller number of taps, we can achieve a considerable improvement in SNR.

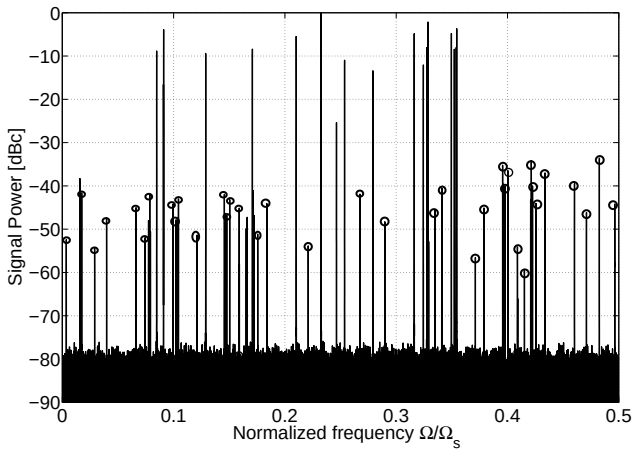

Figure 5.5: *Power spectrum of the uncompensated output* $y[n]$ *with* $Q_H = 16$ *bits and* $Q_L = 2$ *bits. The tones marked with circles are the aliasing components due to the frequency response mismatches. The computed SNR is* 28.3 *dB.*

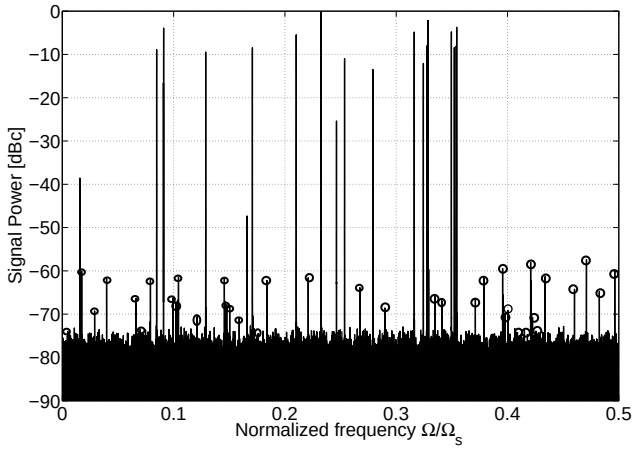

Figure 5.6: *Power spectrum of the compensated output* $y_c[n]$ *using a compensation filter with* 17 *taps (once LMS has been converged). Due to the reduction in the energy of the aliasing components the computed SNR is* 49 *dB thus leading to an approximate improvement of* 21 *dB compared to the uncompensated output.*

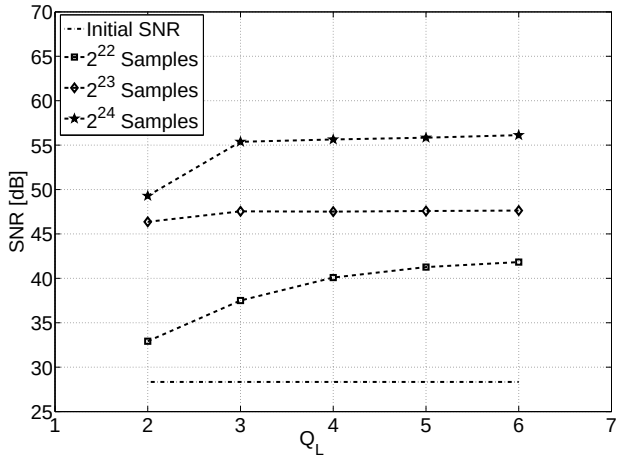

Figure 5.7: *Q_L vs SNR using a compensation filter with* 17 *taps ($Q_H = 16$ bits).*

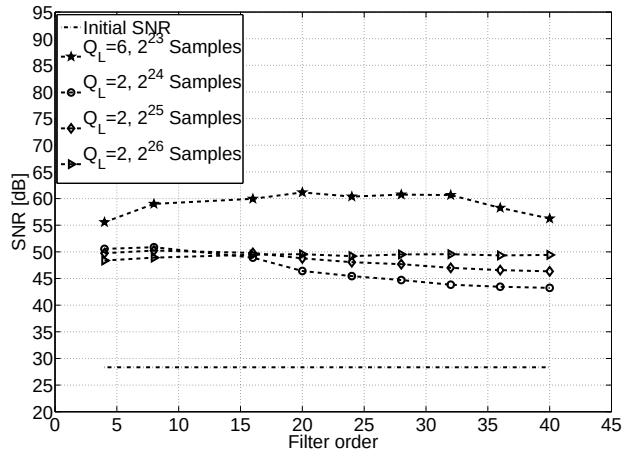

Figure 5.8: *The filter order L of the compensation filter $g_n[l]$ vs SNR using different values of Q_L.*

6

Summary & Concluding Remarks

In this thesis we have investigated the adaptive calibration of frequency response mismatches in time-interleaved ADCs. We have presented the continuous-time, discrete-time, and time-varying system models of a TI-ADC where we have modeled the m-th channel ADC by using a linear time-invariant frequency response $H_m(e^{j\omega})$. The frequency response $H_m(e^{j\omega})$ has been defined to cater for the frequency response mismatches including gain, timing, and bandwidth mismatches. Using these models, we have represented the output of a TI-ADC in two different forms, i.e., first as the sum of a reference signal without mismatches and an error signal due to the mismatches, and second as the output of a time-varying system where with each sampling instant the input signal is convolved with a different impulse response and thus the frequency response mismatches arise. In the former case our calibration philosophy has revolved around adaptively generating an estimated error signal that was subtracted from the TI-ADC output to get the reconstructed input signal. In the latter case we have used an adaptive M-periodic time-varying filter to compensate the frequency response mismatches.

In chapter 3 we have introduced an accurate adaptive blind background calibration technique to calibrate gain (constant magnitude) and timing (linear phase) mismatches in an M-channel TI-ADC. In the first half of this chapter we have first approximated the discrete-time system model introduced in chapter 2 with a first-order Taylor's series expansion. This has helped us to get a unified vector representation for gain and timing mismatch coefficients. In the second half of this chapter, we have presented the details of the blind calibration structure that takes advantage of the slight oversampling of the input signal to estimate and compensate the mismatches. The proposed method has shown significant improvement in the performance of a TI-ADC both with the bandlimited multitone and white Gaussian noise input signals.

In chapter 4 we have presented a fully blind background method to calibrate the frequency response mismatches in a two-channel TI-ADC. By characterizing the frequency

response mismatch between the channel ADCs through the coefficients of a Pth order polynomial has helped us to simply identify those coefficients in order to compensate the mismatches. The unique feature of this structure when compared to the other methods in the literature [63, 73, 75] is its flexibility because it has performed equally well with different channel mismatch models and input signals. However, the extension of this method to an M-channel TI-ADC is an open research question.

An adaptive non-blind background calibration that uses an additional low-resolution reference ADC in combination with a time-varying filter to calibrate frequency response mismatches due to the time-varying behavior of a TI-ADC has been presented in chapter 5. The simulations have shown that, by using a 2-bit ADC as reference and waiting for around 2^{23}, it is possible to adaptively calibrate frequency response mismatches. However the convergence time can be decreased by increasing the resolution of the reference ADC which, however, will increase the total power consumption of the compensated TI-ADC. A possible extension to this non-blind structure, is to use multirate theory such that the time-varying compensation filter $g_n[l]$ may be represented as an M-channel maximally decimated multi-rate filter bank [56]. Furthermore, an implementation on the low rate using polyphase filters can make it more efficient for the digital circuit design.

To summarize, we have found a comprehensive model for time-interleaved ADCs and have analyzed channel mismatch errors. With our background blind and non-blind calibration methods we can precisely identify and compensate the channel mismatches, which significantly improves the performance of a time-interleaved ADC. Therefore, in the future high-rate time-interleaved ADCs can be used for high-resolution applications.

Bibliography

[1] F. Maloberti, "High-speed data converters for communication systems," *IEEE Circuits and Systems Magazine*, vol. 1, no. 1, pp. 26–36, Jan. 2001.

[2] B. Murmann, "Digitally assisted analog circuits," *IEEE Micro*, vol. 26, no. 2, pp. 38–47, Mar. 2006.

[3] B. Murmann, C. Vogel, and H. Koeppl, "Digitally enhanced analog circuits: System aspects," in *Proceedings of IEEE International Symposium on Circuits and Systems, ISCAS, Seattle, WA (USA)*, May 2008, pp. 560–563.

[4] W. C. Black and D. A. Hodges, "Time-interleaved converter arrays," *IEEE Journal of Solid State Circuits*, vol. 15, no. 6, pp. 1024–1029, Dec. 1980.

[5] C. Vogel and H. Johansson, "Time-interleaved analog-to-digital converters: Status and future directions," in *Proceedings of the IEEE International Symposium on Circuits and Systems, ISCAS, Kos (Greece)*, May 2006, pp. 3386–3389.

[6] D. Fu, K. C. Dyer, H.-S. Lewis, and P. J. Hurst, "A digital background calibration technique for time-interleaved analog-to-digital converters," *IEEE Journal of Solid-State Circuits*, vol. 33, no. 12, pp. 1904–1911, Dec. 1998.

[7] K. Dyer, F. Daihong, S. Lewis, and P. J. Hurst, "An analog background calibration technique for time-interleaved analog-to-digital converters," *IEEE Journal of Solid-State Circuits*, vol. 33, no. 12, pp. 1912–1919, Dec. 1998.

[8] H. Jin and E. K. F. Lee, "A digital background calibration technique for minimizing timing-error effects in time-interleaved ADCs," *IEEE Transactions on Circuits and Systems II: Analog and Digital Signal Processing*, vol. 47, no. 7, pp. 603–613, July 2000.

[9] S. Jamal, D. Fu, M. Singh, P. Hurst, and S. Lewis, "Calibration of sample-time error in a two-channel time-interleaved analog-to-digital converter," *IEEE Transactions on Circuits and Systems I: Regular Papers*, vol. 51, no. 1, pp. 130–139, Jan. 2004.

[10] J. Elbornsson, F. Gustafsson, and J.-E. Eklund, "Blind adaptive equalization of mismatch errors in a time-interleaved A/D converter system," *IEEE Transactions on Circuits and Systems I: Regular Papers*, vol. 51, no. 1, pp. 151–158, Jan. 2004.

[11] M. Seo, M. Rodwell, and U. Madhow, "Blind correction of gain and timing mismatches for a two-channel time-interleaved analog-to-digital converter," in *Proceedings of* 39*th IEEE Asilomar Conference on Signals, Systems and Computers, Pacific Grove, California (USA)*, Oct. 2005, pp. 1121–1125.

[12] S. Huang and B. Levy, "Adaptive blind calibration of timing offset and gain mismatch for two-channel time-interleaved ADCs," *IEEE Transactions on Circuits and Systems I: Regular Papers*, vol. 53, no. 6, pp. 1276–1288, June 2006.

[13] V. Divi and G. Wornell, "Blind calibration of timing skew in time-interleaved analog-to-digital converters," *IEEE Journal of Selected Topics in Signal Processing*, vol. 3, no. 3, pp. 509–522, June 2009.

[14] S. Saleem and C. Vogel, "On blind identification of gain and timing mismatches in time-interleaved analog-to-digital converters," in 33*rd International Conference on Telecommunications and Signal Processing, Baden (Austria)*, Aug 2010, pp. 151–155.

[15] ——, "Adaptive blind background calibration of polynomial-represented frequency response mismatches in a two-channel time-interleaved ADC," *IEEE Transactions on Circuits and Systems I: Regular Papers, Accepted for publication*, 2010.

[16] ——, "LMS-based identification and compensation of timing mismatches in a two-channel time-interleaved analog-to-digital converter," in *Proceedings of the* 25*th IEEE Norchip Conference, Aalborg (Denmark)*, Nov. 2007.

[17] C. Vogel, S. Saleem, and S. Mendel, "Adaptive blind compensation of gain and timing mismatches in M-channel time-interleaved ADCs," in *Proceedings of the* 15*th IEEE International Conference on Electronics, Circuits, and Systems, ICECS, St. Julians (Malta)*, Sep. 2008, pp. 49–52.

[18] S. Saleem and C. Vogel, "Adaptive compensation of frequency response mismatches in high-resolution time-interleaved ADCs using a low-resolution ADC and a time-varying filter," in *IEEE International Symposium on Circuits and Systems, ISCAS, Paris (France)*, May/June 2010, pp. 561–564.

[19] W. C. Black, *High speed CMOS A/D conversion techniques.* Ph.D. Dissertation, University of California, Berkeley, Nov. 1980.

[20] N. Kurosawa, H. Kobayashi, K. Maruyama, H. Sugawara, and K. K., "Explicit analysis of channel mismatch effects in time-interleaved ADC systems," *IEEE Transactions on Circuits and Systems I: Fundamental Theory and Applications*, vol. 48, no. 3, pp. 261–271, Mar. 2001.

[21] A. V. Oppenheim, R. W. Schafer, and J. R. Buck, *Discrete-Time Signal Processing.* Prentice Hall, 1999.

[22] *IEEE standard for terminology and test methods for analog-to-digital converters.* IEEE Std 1241 − 2000, June 2001.

[23] S. Haykin, *Adaptive Filter Theory.* Prentice-Hall, 2002.

[24] A. Petraglia and S. Mitra, "Analysis of mismatch effects among A/D converters in a time-interleaved waveform digitizer," *IEEE Transactions on Instrumentation and Measurement*, vol. 40, no. 5, pp. 831–835, Oct. 1991.

[25] A. Petraglia and M. Pinheiro, "Effects of quantization noise in parallel arrays of analog-to-digital converters," in *IEEE International Symposium on Circuits and Systems, ISCAS, London (England)*, vol. 5, May/June 1994, pp. 337–340.

[26] N. Kurosawa, H. Kobayashi, K. Maruyama, H. Sugawara, and K. K., "Explicit formula for channel mismatch effects in time-interleaved ADC systems," in *Proceedings of the* 17*th IEEE Instrumentation and Measurement Technology Conference, IMTC, Baltimore, Maryland (USA)*, vol. 2, May 2000, pp. 763–768.

[27] J. Elbornsson, F. Gustafsson, and J.-E. Eklund, "Analysis of mismatch effects in a randomly interleaved A/D converter system," *IEEE Transactions on Circuits and Systems I: Regular Papers*, vol. 52, no. 3, pp. 465–476, Mar. 2005.

[28] C. Vogel, "The impact of combined channel mismatch effects in time-interleaved ADCs," *IEEE Transactions on Instrumentation and Measurement*, vol. 54, no. 2, pp. 415–427, Feb. 2005.

[29] C. Conroy, D. Cline, and P. Gray, "An 8-b 85-MS/s parallel pipeline A/D converter in 1-μm CMOS," *IEEE Journal of Solid-State Circuits*, vol. 28, no. 4, pp. 447–454, Apr. 1993.

[30] Y. C. Jenq, "Digital spectra of nonuniformly sampled signals: Fundamentals and high-speed waveform digitizers," *IEEE Transactions on Instrumentation and Measurement*, vol. 37, no. 2, pp. 245–251, June 1988.

[31] ——, "Digital spectra of nonuniformly sampled signals: Digital look-up tunable sinusoidal oscillators," *IEEE Transactions on Instrumentation and Measurement*, vol. 37, no. 3, pp. 358–362, Sep. 1988.

[32] ——, "Digital spectra of nonuniformly sampled signals: A robust sampling time offset estimation algorithm for ultra high-speed waveform digitizers using interleaving," *IEEE Transactions on Instrumentation and Measurement*, vol. 39, no. 1, pp. 71–75, Feb. 1990.

[33] ——, "Digital spectra of nonuniformly sampled signals: Theories and applications-measuring clock/aperture jitter of an A/D system," *IEEE Transactions on Instrumentation and Measurement*, vol. 39, no. 6, pp. 969–971, Dec. 1990.

[34] F. A. Marvasti, M. Analoui, and M. Gamshadzahi, "Recovery of signals from nonuniform samples using iterative methods," *IEEE Transactions on Signal Processing*, vol. 39, no. 4, pp. 872–878, Apr. 1991.

[35] F. Marvasti, C. Liu, and G. Adams, "Analysis and recovery of multidimensional signals from irregular samples using non-linear and iterative techniques," in *Proceedings of the IEEE International Symposium on Circuits and Systems, ISCAS,*, vol. 5, May 1992, pp. 2445–2448.

[36] F. A. Marvasti, *Nonuniform Sampling: Theory and Practice*. Kluwer Academic/Plenum Publishers, New York, 2001.

[37] H. Jin and E. K. F. Lee, "A digital technique for reducing clock jitter effects in time-interleaved A/D converter," in *Proceedings of the IEEE International Symposium on Circuits and Systems, ISCAS, Orlando, Florida (USA)*, May 1999, pp. 330–333.

[38] H. Johansson and P. Lowenborg, "Reconstruction of nonuniform sampled bandlimited signals using digital fractional filters," in *IEEE International Symposium on Circuits and Systems, ISCAS, Sydney (Australia)*, May 2001, pp. 593–596.

[39] ——, "Reconstruction of a class of nonuniformly sampled and decimated bandlimited signals," in *IEEE International Symposium on Circuits and Systems, ISCAS. Phoenix-Scottsdale, Arizona (USA)*, vol. 2, 2002, pp. 604–607.

[40] ——, "Reconstruction of nonuniformly sampled bandlimited signals by means of digital fractional delay filters," *IEEE Transactions on Signal Processing*, vol. 50, no. 11, pp. 2757–2767, Nov. 2002.

[41] H. Johansson, P. Lowenborg, and K. Vengattaramane, "Reconstruction of two-periodic nonuniformly sampled signals using polynomial impulse response time-varying FIR filters," in *Proceedings of the IEEE International Symposium on Circuits and Systems, ISCAS, Kos (Greece)*, May 2006, pp. 2993–2996.

[42] ——, "Least-squares and minimax design of polynomial impulse response FIR filters for reconstruction of two-periodic nonuniformly sampled signals," *IEEE Transactions on Circuits and Systems I: Regular Papers*, vol. 54, no. 4, pp. 877–888, Apr. 2007.

[43] S. Jamal, D. Fu, N.-J. Chang, P. Hurst, and S. Lewis, "A 10-b 120-MSample/s time-interleaved analog-to-digital converter with digital background calibration," *IEEE Journal of Solid-State Circuits*, vol. 37, no. 12, pp. 1618–1627, Dec. 2002.

[44] J. Elbornsson and J.-E. Eklund, "Blind estimation of timing errors in interleaved AD converters," in *Proceedings of the IEEE International Conference on Acoustics, Speech, and Signal Processing, ICASSP, Salt Lake City, Utah (USA)*, vol. 6, May 2001, pp. 3913–3916.

[45] J. Elbornsson, K. Folkesson, and J.-E. Eklund, "Measurement verification of estimation method for time errors in a time-interleaved A/D converter system," in *IEEE International Symposium on Circuits and Systems, ISCAS, Phoenix-Scottsdale, Arizona (USA)*, vol. 3, May 2002, pp. 129–132.

[46] J. Elbornsson, F. Gustafsson, and J.-E. Eklund, "Blind equalization of time errors in a time-interleaved ADC system," *IEEE Transactions on Signal Processing*, vol. 53, no. 4, pp. 1413–1424, Apr. 2005.

[47] J. Pereira, P. Girao, and A. Serra, "An FFT-based method to evaluate and compensate gain and offset errors of interleaved ADC systems," *IEEE Transactions on Instrumentation and Measurement*, vol. 53, no. 2, pp. 423–430, Apr. 2004.

[48] R. Prendergast, B. Levy, and P. Hurst, "Reconstruction of band-limited periodic nonuniformly sampled signals through multirate filter banks," *IEEE Transactions on Circuits and Systems I: Regular Papers*, vol. 51, no. 8, pp. 1612–1622, Aug. 2004.

[49] M. Seo, M. Rodwell, and U. Madhow, "Blind correction of gain and timing mismatches for a two-channel time-interleaved analog-to-digital converter: Experimental verification," in *Proceedings of the IEEE International Symposium on Circuits and Systems, ISCAS, Kos (Greece)*, May 2006, pp. 3394–3397.

[50] C. Vogel, D. Draxelmayr, and F. Kuttner, "Compensation of timing mismatches in time-interleaved analog-to-digital converters through transfer characteristics tuning," in *47th Midwest Symposium on Circuits and Systems, MWSCAS, Hiroshima (Japan)*, vol. 1, July 2004, pp. 341–344.

[51] C. Vogel, "A frequency domain method for blind identification of timing mismatches in time-interleaved ADCs," in *24th IEEE Norchip Conference, Linkoping (Sweden)*, Nov. 2006, pp. 45–48.

[52] S. Tertinek and C. Vogel, "Reconstruction of two-periodic nonuniformly sampled band-limited signals using a discrete-time differentiator and a time-varying multiplier," *IEEE Transactions on Circuits and Systems II: Express Briefs*, vol. 54, no. 7, pp. 616–620, July 2007.

[53] ——, "Reconstruction of nonuniformly sampled bandlimited signals using a differentiator-multiplier cascade," *IEEE Transactions on Circuits and Systems I: Regular Papers*, vol. 55, no. 8, pp. 2273–2286, Sep. 2008.

[54] S. Huang and B. Levy, "Blind calibration of timing offsets for four-channel time-interleaved ADCs," *IEEE Transactions on Circuits and Systems I: Regular Papers*, vol. 54, no. 4, pp. 863–876, Apr. 2007.

[55] V. Divi and G. Wornell, "Scalable blind calibration of timing skew in high-resolution time-interleaved ADCs," in *Proceedings of the IEEE International Symposium on Circuits and Systems, ISCAS, Kos (Greece)*, May 2006, p. 3393.

[56] P. P. Vaidyanathan, *Multirate Systems and Filter Banks*. Prentice-Hall Signal Processing Series, 1993.

[57] Y. C. Jenq, "Perfect reconstruction of digital spectrum from nonuniformly sampled signals," *IEEE Transactions on Instrumentation and Measurement*, vol. 46, no. 3, pp. 649–652, June 1997.

[58] C. Vogel, D. Draxelmayr, and G. Kubin, "Spectral shaping of timing mismatches in time-interleaved analog-to-digital converters," in *IEEE International Symposium on Circuits and Systems, ISCAS, Kobe (Japan)*, May 2005, pp. 1394–1397.

[59] C. Vogel, *Modeling, identification and compensation of channel mismatch errors in time-interleaved analog-to-digital converters*. Ph.D. Dissertation, Graz University of Technology, Austria, July 2005.

[60] C. Vogel and G. Kubin, "Modeling of time-interleaved ADCs with nonlinear hybrid filter banks," *AEU-International Journal of Electronics and Communications*, vol. 59, no. 5, pp. 288–296, July 2005.

[61] ——, "Analysis and compensation of nonlinearity mismatches in time-interleaved ADC arrays," in *Proceedings of the IEEE International Symposium on Circuits and Systems, ISCAS, Vancouver (Canada)*, vol. 1, May 2004, pp. 593–596.

[62] Y. Huang, *Blind Calibration for Time-Interleaved Analog-to-Digital Converters*. Ph.D. Dissertation, University of California, Davis, 2006.

[63] M. Seo, M. Rodwell, and U. Madhow, "Generalized blind mismatch correction for two-channel time-interleaved A-to-D converters," in *IEEE International Conference on Acoustics, Speech and Signal Processing, ICASSP, Honolulu, Hawaii (USA)*, vol. 3, Apr. 2007, pp. 1505–1508.

[64] P. Satarzadeh, B. Levy, and P. Hurst, "Bandwidth mismatch correction for a two-channel time-interleaved A/D converter," in *IEEE International Symposium on Circuits and Systems, ISCAS, New Orleans, LA (USA)*, May 2007, pp. 1705–1708.

[65] P. Satarzadeh, B. C. Levy, and P. J. Hurst, "Adaptive semi-blind calibration of bandwidth mismatch for two-channel time-interleaved ADCs," *IEEE Transactions on Circuits and Systems I: Regular Papers*, vol. 56, no. 9, pp. 2075–2088, Sep. 2009.

[66] T.-H. Tsai, P. Hurst, and S. Lewis, "Bandwidth mismatch and its correction in time-interleaved analog-to-digital converters," *IEEE Transactions on Circuits and Systems II: Express Briefs*, vol. 53, no. 10, pp. 1133–1137, Oct. 2006.

[67] M. Seo, M. Rodwell, and U. Madhow, "Comprehensive digital correction of mismatch errors for a 400-MSamples/s 80-dB SFDR time-interleaved analog-to-digital converter," *IEEE Transactions on Microwave Theory and Techniques*, vol. 53, no. 3, pp. 1072–1082, Mar. 2005.

[68] K. Asami, "Technique to improve the performance of time-interleaved A-D converters," in *Proceedings of the IEEE International Test Conference, ITC, Austin, TX (USA)*, Nov. 2005, pp. 851–857.

[69] S. Mendel and C. Vogel, "A compensation method for magnitude response mismatches in two-channel time-interleaved analog-to-digital converters," in 13*th IEEE International Conference on Electronics, Circuits and Systems, ICECS, Nice (France)*, Dec. 2006, pp. 712–715.

[70] ——, "On the compensation of magnitude response mismatches in M-channel time-interleaved ADCs," in *IEEE International Symposium on Circuits and Systems, ISCAS, New Orleans (USA)*, May 2007, pp. 3375–3378.

[71] C. Vogel and S. Mendel, "A flexible and scalable structure to compensate frequency response mismatches in time-interleaved ADCs," *IEEE Transactions on Circuits and Systems I: Regular Papers*, vol. 56, no. 11, pp. 2463–2475, Nov. 2009.

[72] H. Johansson and P. Löwenborg, "A least-squares filter design technique for the compensation of frequency-response mismatch errors in time-interleaved A/D converters," *IEEE Transactions on Circuits and Systems II: Express Briefs*, vol. 55, no. 6, pp. 1154–1158, Nov. 2008.

[73] T.-H. Tsai, P. J. Hurst, and S. H. Lewis, "Correction of mismatches in a time-interleaved analog-to-digital converter in an adaptively equalized digital communication receiver," *IEEE Transactions on Circuits and Systems I: Regular Papers*, vol. 56, no. 2, pp. 307–319, Feb. 2009.

[74] M. Seo and M. Rodwell, "Generalized blind mismatch correction for a two-channel time-interleaved ADC: Analytic approach," in *IEEE International Symposium on Circuits and Systems, ISCAS, New Orleans (USA)*, May 2007, pp. 109–112.

[75] H. Johansson, "A polynomial-based time-varying filter structure for the compensation of frequency-response mismatch errors in time-interleaved ADCs," *IEEE Journal of Selected Topics in Signal Processing*, vol. 3, no. 3, pp. 384–396, June 2009.

[76] W. Kester, *Mixed-Signal and DSP Design Techniques*. Newnes, 2003.

[77] R. Khoini-Poorfard, L. B. Lim, and D. A. Johns, "Time-interleaved oversampling A/D converters: Theory and practice," *IEEE Transactions on Circuits and Systems II: Analog and Digital Signal Processing*, vol. 44, no. 8, pp. 634–645, Aug. 1997.

[78] E. Kreyszig, *Advanced Engineering Mathematics*. 8th Ed., John-Wiley and Sons, 1998.

[79] S. Saleem, "Adaptive blind calibration techniques for gain-timing and generalized mismatch models in time-interleaved analog-to-digital converters," *Technical Report, Signal Processing and Speech Commuincation Laboratory, Graz University of Technology, Austria*, 2008.

[80] ——, "A comparative analysis of blind calibration techniques for time-interleaved ADCs," in *Proceedings of* 16*th Austrian Workshop on Microelectronics, AustroChip, Linz (Austria)*, Oct. 2008, pp. 33–37.

[81] B. Widrow and S. D. Stearns, *Adaptive Signal Processing*. Prentice-Hall, 1985.

[82] E. Bjarnason, "Analysis of the filtered-X LMS algorithm," *IEEE Transactions on Speech and Audio Processing*, vol. 3, no. 6, pp. 504–514, Nov. 1995.

[83] A. V. Oppenheim and A. Willsky, *Signals and Systems*. Prentice Hall, 1983.

[84] C. Vogel, "A signal processing view on time-interleaved ADCs," pp. 61–78, 2010.

[85] D. Marelli, K. Mahata, and M. Fu, "Linear LMS compensation for timing mismatch in time-interleaved ADCs," *IEEE Transactions on Circuits and Systems I: Regular Papers*, vol. 56, no. 11, pp. 2476–2486, Nov. 2009.

[86] K. Poulton, R. Neff, B. Setterberg, B. Wuppermann, T. Kopley, R. Jewett, J. Pernillo, C. Tan, and A. Montijo, "A 20-GS/s 8-bit ADC with a 1 MB memory in 0.18μm CMOS," in *IEEE International Solid-State Circuits Conference, Digest of Technical papers, ISSCC, San Francisco, CA (USA*, vol. 1, Feb. 2003, pp. 318–496.

[87] T. Sundstroem, B. Murmann, and C. Svensson, "Power dissipation bounds for high-speed Nyquist analog-to-digital converters," *IEEE Transactions on Circuits and Systems I: Regular Papers*, vol. 56, no. 3, pp. 509–518, Mar. 2009.

[88] Y. C. Lim, Y. X. Zou, J. W. Lee, and S. C. Chan, "Time-interleaved analog-to-digital converter (TIADC) compensation using multichannel filters," *IEEE Transactions on Circuits and Systems I: Regular Papers*, vol. 56, no. 10, pp. 2234–2247, October 2009.

[89] H. Johansson and P. Löwenborg, "Reconstruction of nonuniformly sampled bandlimited signals by means of time-varying discrete-time FIR filters," *EURASIP Journal on Applied Signal Processing*, vol. 2006, 2006. [Online]. Available: http://www.hindawi.com/journals/asp/2006/064185.abs.html